Multifunctional Nano MOF Particle for Anticancer Drug Delivery

by

Feng Zhao

A thesis
presented to the University of Waterloo
in fulfillment of the
thesis requirement for the degree of
Master of Applied Science
in
Chemical Engineering (Nanotechnology)

Waterloo, Ontario, Canada, 2021

Author’s Declaration

I hereby declare that I am the sole author of this thesis. This is a true copy of the thesis, including any required final revisions, as accepted by my examiners.

I understand that my thesis may be made electronically available to the public.

Abstract

Nano metal organic framework materials (MOFs) are a new class of porous materials these years. They have attracted much attention due to their wide applications in the fields of drug delivery [1]. Based on the structural advantages of MOFs, the active sites of ligands can control the interaction of drugs with biological systems [2]. At the same time, weaker coordination bonds ensure biodegradability [1]. A self-assembly cell-penetrating peptide, NP1, for siRNA and drug delivery systems has been developed in our group. In this thesis, NP1 peptide was modified to introduce targeting function. Peptide-based drug and siRNA vectors have many advantages, such as biodegradability, high transmembrane efficiency, and endosome escape ability [3,4]. Doxorubicin (anti-tumor drug) can be loaded in porphyrin-MOFs which have a large photosensitizer loading. Peptide functionalized nano metal organic framework materials can be used for drug delivery and photodynamic therapy to target anti-tumor drug and photosensitizer-containing MOF particles to tumor cells.

Acknowledgments

Time flies and the two-year intense and fulfilling master's program is about to end in no time. I would like to thank the Department of Chemical Engineering of the University of Waterloo for the opportunity to study, and also thank Mitacs and our partner company for their financial support for my graduate program. During the two years of study, not only I got guidance and help from many professors and colleagues in my studies, I also felt the kindness and care of my friends in daily life. We have experienced one of the most influential pandemics in human history together. It is an unforgettable and precious experience of my life to persist in doing postgraduate studies during this difficult period. As my MASc program is about to be completed, I would like to express my sincerest gratitude to all the people and organizations who have given me support, help, and encouragement during this period.

First of all, I want to show my greatest appreciation to my mentor, Prof. Pu Chen, for giving me the opportunity to do research in his group. From the topic selection, conception, writing and finalization of the thesis, Professor Chen gave me careful guidance and enthusiastic help, so that my graduation thesis can be completed smoothly. Professor Chen's

serious and responsible work attitude, academic research spirit, and rigorous style of study are all worthy of my lifelong learning.

Secondly, I would like to thank Professor Guang Chen, Dr. Lei Zhang, and Yuanchao for their help and inspiration in the process of my project design and experimental analysis. Thanks to Dr. Sheng Lu and Dr. Xiaoxia Han for guiding me in multiple experimental technologies. Thanks to Jiao Yuxiao, Han Mei, and other colleagues in the research group for their help during my experiments.

I would also like to thank the members of my reading committee, Prof. Boxin Zhao from the Department of Chemical Engineering, and Prof. Pavle Radovanovic from the Department of Chemistry for their time and constructive feedback in completing this thesis.

Most importantly, I must express my deepest gratitude to my mother for her unremitting support and encouragement throughout my study, research and writing of this thesis.

Table of Contents

List of Figures

List of Tables

Chapter 1 Introduction

1.1 Overview

The existence of cancers, which are also called malignant tumors, seriously endangers human life and health. Tumor refers to a local mass formed by the abnormal proliferation of cells in local tissues under the action of various tumor-causing factors. [5] Malignant tumors can destroy the structure and function of tissues and organs. Patients may eventually die due to organ failure. [6] Chemotherapy is the mainstream treatment method these years. However, due to the disadvantages of poor drug stability, low solubility, large side effects, easy metabolism, no targeting and easy removal during the treatment process, the effective utilization rate of drugs in the treatment of tumors is relatively low.

Nanomedicine defined as nanotechnology applications in medicine is a new field of science and technology, it has great potential in clinical practice for the treatment of various diseases. One of the main goals of nanomedicine is to synthesize suitable drug carriers for anticancer drug delivery. [7, 8] This kind of drug carriers can effectively cross the physiological barrier and accumulate in the diseased position and can continuously release the drug to treat the disease with relatively slight side effects [9]. With the rapid development of nanotechnology and oncology medicine, people have designed a variety of drug carriers that can help realize the effective use of drugs, mainly including organic

nanoparticles (liposomes, polymer nanoparticles, micelles, dendrimers) and inorganic nanoparticles (iron oxide, quantum dots, gold, mesoporous silica, metal organic framework). [10, 11]

Metal organic frameworks (MOFs), also known as porous coordination polymers, are a class of crystalline porous materials composed of metal ions/clusters and organic linkers [12]. Through selecting suitable organic ligands and metal elements, people can synthesize MOFs with different morphologies, sizes, specific functions and specific pore size distributions [13]. Because of its wide application in biosensing, drug delivery and other fields, MOF has attracted much attention and has been sought after by many researchers and applied in nanomedicine. [14] The application of nano metal organic framework materials in drug therapy is closely related to the material's biocompatibility, degradability, sustained release of drug loading and drug targeted delivery. The size and morphology can be reasonably adjusted to obtain biocompatible materials with an average particle size in nano scale through effective methods such as selection of framework material ligands or temperature control. Compared with conventional drug carriers, nano drug carriers can easier traverse tissues and biomembrane structures. They can make the drugs accumulate in the lesion, thereby greatly improving the drug delivery ratio and utilization rate. This is because the hydrodynamic diameter of the long-circulating nanoparticles exceeds the renal clearance threshold. [15] These nanoparticles preferentially penetrate the tumor tissue through the permeable tumor

blood vessels and then remain in the tumor bed due to reduced lymphatic drainage. [16] This process is called enhancement permeability and retention (EPR) effect. [17,18] In addition, weaker coordination bonds ensure that MOFs are biodegradable. [19] These excellent characteristics make MOF nanoparticle an ideal platform for clinical oncology and disease treatment. In cancer chemotherapy, effective drug encapsulation can reduce the death of normal cells, while controlled release can maintain the concentration of the drug in the blood for a long time, thereby improving the patient's adaptability to the drug and improving the therapeutic effect.[20] So far, researchers have developed many stimulus response strategies to control the delivery of drugs, such as pH, photon signals, redox reagents, columnar aromatics, temperature, enzymes, and nucleic acids to control the effective release of drugs.[21] For drug-loading platforms, the external stimulus conditions of the MOF-based stimulus-response release system mainly include pH, electric field, biomolecules, magnetic field, temperature, ions, pressure, light, etc.[22-27]

At present, the commonly used cancer treatment methods include radiotherapy, chemotherapy and surgical resection. [28] Traditional treatment methods such as chemotherapy and radiotherapy have shortcomings such as strong side effects and easy recurrence, so the treatment of cancer often fails to achieve the expected results [29]. In recent years, research of photodynamic therapy (PDT) has made good progress in the treatment of cancer. With laser irradiation of a specific wavelength, photosensitizers can produce reactive oxygen species (ROS), leading to cell apoptosis and necrosis, thereby

achieving the precision treatment on cell level. [30] Porphyrin is a common anti-cancer photosensitizer, which is used in photodynamic therapy in medicine. [31] It is a type of conjugated skeleton macrocyclic compound formed by connecting 4 pyrrole rings through a methane group. In the molecular structure of porphyrin, the 8 β positions and 4 meso hydrogen atoms of the 4 pyrrole rings can be replaced by other groups to generate various porphyrin derivatives. It not only has unique physiological activities but also has a great affinity with cancer cells. [32] Although photodynamic therapy can selectively kill cancer cells by positioning and irradiating photosensitizers to reduce collateral damage to normal tissues, photosensitizers cannot accurately target tumor cells by themselves [33]. Therefore, the targeted delivery of anti-cancer drugs is another focus of research.

To improve the anti-tumor efficiency of drugs, one of the most used strategies is to target cancer cells with molecular ligands that are specifically overexpressed in tumor tissues. Receptor-mediated endocytosis depends on specific ligands that can recognize specific receptors found in the cell membrane. [34] Folic acid (FA), a small molecule commonly referred to as vitamin B9, is an important substance in nucleic acid production, cell division, and cell metabolism [35, 36]. Folate receptors (FRs) are overexpressed in many human cancers, including ovarian cancer, kidney cancer, breast cancer, etc. In addition, the density of folate receptors increases when cancer worsens, so folic acid can be used for tumor targeted therapy. [36] However, FA is also a nutrient required for cell activities and may promote tumor cell growth. This is because the high

levels of DNA replication in cancer tissues require a large amount of folic acid for continued tumor growth [37]. Some substances have molecular structures similar to folic acid and can also be recognized by folate receptors overexpressed by cancer cells. Methotrexate (MTX) is such a structural analogue of folic acid, which is widely used to treat a variety of cancers or severe and drug-resistant forms of autoimmune diseases. As a drug, MTX has a pleiotropic mechanism of action, among which effective anti-metabolic and anti-proliferative effects make MTX can be used in anti-cancer therapy. MTX can guide the drugs bound to it to specific molecular target, and selectively deliver drug molecules to folate receptor expressing cancer cells. It is considered to be the cornerstone of antifolate therapy for the treatment of a variety of malignant tumors. MTX is highly ionized and usually hydrophilic, and it is difficult to penetrate biological barriers [38-41]. Therefore, MTX needs to be loaded into a carrier to help it play a targeting role on folate receptors and kill tumor cells.

Self-assembled systems have attracted great attention due to their great application potential in energy, biomedicine, and nanotechnology. Peptides composed of amino acids are one of the most popular programmable molecular structures. [42] Due to the different assembly mechanisms, the structure of self-assembled peptides has different morphologies, which reflects its application prospects in the field of drug packaging and targeted delivery. [43,44] In fact, like the MTX mentioned above, it is difficult for most drugs and their peptide carriers to directly enter the cell membrane, which causes most

drugs to be trapped in endosomes through endocytosis. [45-47] There is a class of amphiphilic cells, penetrating peptides (CPPs), which retain the self-assembly function, and the specific amino acid sequence exposed on the periphery makes it more permeable to the biomembrane structure [48-50]. These peptides have been extensively studied as carriers of siRNA or drug to improve the retention (EPR) effect and intracellular delivery efficiency. [51,52] Our group has developed a CPP, NP1 (StearylHHHHHHHHHHHHHHHHRRRRRRRR-NH2), aiming to provide highly efficient siRNA and drug delivery. [53,54] NP1 peptide generally possesses an overall positive charge and has an amphiphilic structure. Arginine residues show strong binding affinity to cell membranes because they can provide the positive charge, and then facilitate the cell membrane penetration function of CPPs [55-57]. The hydrophobic interaction provided by stearic acid moiety and the histidine protonation makes NP1 can self-assemble and disassemble triggered by pH value. By arranging amino acids to form specific peptide sequences or chemically modified, CCPs can also become tumor-targeting peptides. [58] For example, RV24, an amphipathic tumor penetrating peptide, can carry drugs to target T98G, HepG2 and Hela cells. [59] In this thesis, an MTX molecule was connected to the NP1 peptide and form an NP1-derived peptide named NPKMTX, which could target to folate receptor and also act as a pro-drug of MTX. Because nano MOFs can be surface modified [60-62], using peptide to modify nano MOFs are feasible, enabling them to help deliver the anticancer drug to tumors.

In addition to MTX, there are some other drugs commonly used in the research of anti-cancer drug delivery. The use of a single anti-cancer drug is easy to produce drug resistance, so a dual-drug delivery method was adopted to further reduce drug resistance while improving chemical lethality. Doxorubicin (DOX) is an anti-tumor drug that can inhibit the synthesis of RNA and DNA. [63] In many drug delivery research reports, it is often selected as a model drug to test the carrier's ability to load and release drugs. [64-67]

In summary, in this research, a nano-MOF drug-carrying platform that can simultaneously deliver photosensitizers and anti-cancer drugs to accurately perform chemotherapy and photodynamic therapy in cancer cells with high folate receptor expressing was designed. Meso-tetra(4-carboxyphenyl) porphyrin (TCPP) is often used as a photosensitizer in biomedicine and biomimetic due to its structural properties. It can produce ROS to kill cancer cells with irradiation of specific wavelengths light [68]. Therefore, we chose PCN-224 as the MOF platform in this research. PCN-224 is a MOF structure composed of the Zr_6 cluster as the node and TCPP as the linker. PCN is the short of porous coordination network, so PCN-224 has great potential for drug loading and delivery. It is well known that the shape and size of nano MOF particles will affect the loading of drugs and cell uptake. Therefore, it is very important to control the size of MOFs in the synthesis process. Firstly, according to literature reports, we conducted the synthesis of nano-PCN-224. Subsequently, the PCN-224 nanoparticles were loaded with drugs to form the Dox@PCN-224 (DP) complex. Furthermore, DP was modified with

NPKMTX peptide to construct a peptide-functionalized nano-drug carrier system DOX@PCN-224-NPKMTX (DPN). NPKMTX peptide-functionalized PCN-224 MOF can specifically recognize tumor cells by binding to the folate receptor when in contact with tumor cells. Because of the weakly acidic tumor microenvironment, when DOX@PCN-224-NPKMTX enters the cell, the lower pH value will trigger the disassembly of NPKMTX peptide and then the release of Dox. The NPKMTX peptide also releases MTX during the degradation process in lysosome, thereby inducing tumor cell apoptosis through dual-drug chemotherapy. In addition, the TCPP in PCN-224 can generate reactive oxygen species (ROS) through laser irradiation of a specific wavelength, which will further increase the mortality of tumor cells. In this research project, starting from developing peptide-functionalized MOFs for drug encapsulation and controlled release and targeted delivery, the Dox loading PCN-224 nano MOF functionalized by NPKMTX peptide was designed to achieve targeted drug delivery and photodynamic therapy of tumors, which provides a new perspective for drug stimuli-responsive release and targeted therapy of cancer.

1.2 Objectives

The general objective of this project is to design a multifunctional nano MOF particle for anticancer drug delivery.

- Modification of NP1 with MTX for targeting to folate receptor.
- Synthesis of PCN-224 nano MOF particles and loading dox inside
- Coating PCN-224 nanoparticles with NPKMTX peptide to construct a multifunctional MOF nano drug delivery platform
- Successful disassembly of NPKMTX peptide and release of Dox from DPN complexes triggered by pH.
- Conducting in vitro tests of cell cytotoxicity, cellular uptake of PCN MOF complexes.
- Observation of drug distribution at the subcellular level.

1.3 Outline

There are five chapters in this thesis.

Chapter 1 is the overview of the project. Firstly, it includes an introduction to metal organic framework (MOF) as drug delivery carriers, photodynamic therapy (PDT), folic acid structural analogue MTX, cell penetration peptide NP1 and their anticancer activities. In addition, the overall design idea and strategy of this research project are discussed briefly. The objectives and outline of the thesis are also provided in this chapter.

Chapter 2 gives a brief review of current advances in the development of anticancer therapy, application of MOF materials and self-assembling peptides in anticancer therapy.

Chapter 3 describes the methodology in synthesis and physicochemical characterizations of designed NPKMTX peptide-functionalized PCN-224 nano MOF drug carrier. Fluorescence spectroscopy, dynamic light scattering (DLS), circular dichroism spectroscopy (CDs), atomic force microscopy (AFM), scanning electronic microscopy (SEM) and Fourier-transform infrared spectroscopy (FTIR) are used to characterize formulation of peptide aggregation, peptide secondary structure, nanoparticle size and zeta potential, drug loading efficiency and release profile, peptide modification efficiency

and morphology respectively. Results of each experiment are discussed accordingly, and an overall conclusion of the chapter is presented in the end.

Chapter 4 describes the methodology in nanoparticles uptake and drug release process in vitro. CCK-8 assay, fluorescence-activated cell sorting (FACS) and confocal laser scanning microscope (CLSM) are used to determine cytotoxicity, cellular uptake, drug distribution at the subcellar level and targeting function for the performance of designed multifunctional nano MOF particles. Results of each experiment are discussed accordingly, and an overall conclusion of the chapter is presented in the end.

Chapter 2 Literature Review

2.1 Cancer

Cancer, also called a malignant tumor, is a highly fatal disease worldwide. The combined effect of genetic factors and environmental factors leads to the onset of malignant tumors [69]. Firstly, gene mutations create pre-requisite conditions for cell carcinogenesis; secondly, various carcinogenic factors produce cancer-causing substances under the action of complex conditions in the body, which constitute the inducement of gene mutation; finally, the production of oncogenes may be related to the body's immune function imbalance [70-72]. Malignant tumors will grow rapidly and indefinitely and cannot be fundamentally controlled. Cancer cells can be transferred to normal biological structures, causing other normal physiological activities in the body to be out of balance, thereby inducing cancer in other parts of the body. Individuals suffering from cancer diseases should be treated promptly and effectively, and anti-cancer drugs should be used according to the area where cancer cells exist and the cycle state. Anti-cancer drugs are roughly divided into four categories: drugs that directly damage the structure and function of DNA; drugs that interfere with DNA synthesis; drugs that fight cancer cell mitosis; drugs based on cancer biological mechanisms [73-76]. Nowadays, biological therapy, body immunotherapy, chemotherapy and new target drug research have made great progress, and the development of anti-tumor drugs has entered a new era [77,78].

2.1.1 Tumor markers

Tumor markers are a class of substances that reflect the existence or growth of tumors. They exist in the blood, body fluids, cells or tissues of patients, and can be expressed on tumor cells and normal cells. [79,80] They have high sensitivity and specificity. Tumor-specific immune response caused and produced by abnormalities can be determined by methods such as biochemistry, immunology and molecular biology. Tumor markers are mainly used in the diagnosis of malignant tumors, evaluation of treatment effects, recurrence diagnosis and prognostic analysis. [81] Tumor marker mainly exists in serum and serous effusion, the collection of tumor markers is easy and causes less trauma [82], so it is a hot spot in the current diagnosis research of malignant tumors.

Currently, a variety of tumor markers have been used for clinical diagnosis, they can be classified as serum tumor markers and cellular tumor markers. Serum tumor markers include carcinoembryonic antigens, enzymes, hormones and glycoproteins, and cellular tumor markers include oncogenes and cell surface tumor antigens, most of which have been used for clinical testing. Tumor markers with high sensitivity and specificity can be used to detect and monitor tumor diseases. [83] Therefore, the early diagnosis of tumors through the detection of tumor markers has attracted widespread scientific attention.

2.1.2 Dox application in anticancer chemotherapy

Doxorubicin (DOX) has a strong cytotoxic effect and can interfere with DNA and inhibit nucleic acid synthesis. It is a drug that acts on the chemical structure of DNA [84]. Dox has a broad-spectrum anti-tumor effect, both benign tumors and malignant tumors are within its treatment range. However, from the current research, because doxorubicin has a strong cytotoxic effect [85], it is necessary to pay attention to its side effects during clinical administration. For example, it will affect the hematopoietic function of the bone marrow and decrease the immune function, which may induce a variety of illnesses [86]. Therefore, dox cannot be used continuously for a long time. It should be used in combination with other drugs or rotation, so that the clinical efficacy can be best guaranteed, and the development of drug resistance could also be minimized at the same time. [87] The use of nanomaterials as carriers is very suitable for the delivery of chemotherapeutic drugs like dox in cancer treatment [88]. This is because nanomaterials as a carrier platform have strong permeability and retention delay effects in the treatment of tumors and can passively target tumor cells. The development results of nano diagnosis and treatment have already been applied to the clinic, advanced materials technology has developed rapidly in recent years, and many higher levels of functionally modified nanoparticle platforms are being researched and utilized [89].

Since the release rate and maximum cumulative rate of doxorubicin hydrochloride are affected by pH, it shows a sustained release characteristic. For example, Guoping Li with

his colleagues have designed a DOX-conjugated CQD-based nano sponge for tumor intracellular pH-triggered DOX release and imaging [107]. It is verified that the prepared nano sponges showed excellent pH-triggered drug release performance in the simulated tumor intracellular microenvironment, which can increase the persistence and stability of the drug in the cell. This could help reduce the amount of medicine used for the disease and reduce or avoid the toxic side effects caused by the medicine in the case that is most conducive to the treatment of the disease.

2.1.3 Photodynamic therapy treating cancer

Photodynamic Therapy (PDT) is an emerging technology developed in recent years, which has made a breakthrough in tumor treatment. Its principle is that when the photosensitizer enters the cell, the photosensitizer will be activated by the specific wavelength laser irradiation. [90,91] Under the induction of the activated photosensitizer, reactive oxygen species (ROS) are generated in the cell. [91] ROS will oxidize with adjacent biological macromolecules, thereby destroying the structure and function of the cell, producing cytotoxicity and poisoning the cancer cells, leading to cell damage and death, and then the tumor mass will gradually decrease and disappear. [92,93] It is a new treatment method that effectively kills cancer cells by combining photosensitizer and laser irradiation. Due to the generation of cytotoxic reactive oxygen species (ROS), photodynamic therapy (PDT) using porphyrin has been approved for the treatment of a variety of solid tumors. However, there are still some defects like low physiological solubility and lack of selectivity for tumor sites limiting the application of PDT in the clinic. [94] In 1978, Dougherty et al.1 reported the first clinical case of PDT in a patient with metastatic breast cancer to the skin. The first clinical case of PDT was reported by Dougherty et al. in 1978 to treat a patient with metastatic breast cancer to the skin. [95]

However, the tumor is easy to recur with PDT treatment only. Xin et al. developed a drug carrier system based on β-CD functionalized carbon quantum dots (CQD) using anticancer chemotherapy drugs (DOX) and photosensitizer (5-ALA) to

inhibit breast cancer cells through chemo photodynamic therapy. [96] The photosensitizer as a carrier material itself can enhance the treatment effect of cancer, and the photodynamic fluorescence diagnosis technology can be used to detect early tumors or precancerous lesions and use fluorescence imaging to guide the laser to accurately irradiate tumor tissues. Compared with traditional cancer treatments, PDT has many advantages, including minimally invasive, fast recovery, precise tumor targeting, minimal systemic toxicity, and the feasibility of repeated treatments, etc.

2.2 Overview of metal organic framework

Metal organic frameworks (MOFs), also known as porous coordination polymers, are a class of crystalline porous materials and metal ions/clusters composed of organic linkers [97]. They have received extensive attention in the past decades and have achieved great development. Due to the diversity of its crystal structure properties, adaptability and ultra-high surface area, MOFs have become a highly versatile platform in many fields such as gas adsorption and separation, chemical sensing and biomedicine with potential application prospects [98]. By adjusting the type of functional group on the ligand and the type of metal salt, MOFs can be synthesized through the evaporative solvent method, diffusion method (also can be finely divided into gas phase diffusion, liquid phase diffusion, gel diffusion, etc.), hydrothermal or solvothermal method, ultrasonic and microwave method etc. [99]. Among these synthesis methods, hydrothermal or solvothermal methods are the most important and commonly used. Hydrothermal or solvothermal methods belong to the category of liquid-phase chemical methods, which refer to chemical synthesis methods in a sealed pressure vessel, using water as a solvent, with high temperature and high-pressure conditions [43]. MOFs materials with different morphologies, sizes, specific functions and specific pore size distributions can be synthesized through selecting appropriate organic ligands and metal elements, clarifying the synthesis mechanism of MOFs,

controlling the synthesis conditions and selecting appropriate nucleation and growth methods. [44]

2.2.1 Application of MOF-based materials in drug delivery research

The application of nano-metal-organic framework materials in drug therapy is closely related to the material's compatibility, degradability, drug loading, sustained release and targeted delivery. The size and morphology can be adjusted reasonably through the selection of framework material ligands, temperature control and other effective ways to obtain biocompatible materials with an average particle size of less than 200nm [100]. Compared with conventional drug carriers, it is easier for nano drug carriers to traverse bio tissues. They make the distribution of the drugs more widely, which can greatly improve the drug delivery rate and utilization rate. In addition, the weaker coordination bond ensures that MOFs are biodegradable. These excellent properties make MOFs an ideal platform for the treatment of clinical tumors and diseases [101].

MOFs materials should be biocompatible in biological applications. At present, Fe, Zn, Zr, Mn, Mg and Cu are widely used in the construction of MOFs due to their lower toxicity determined using oral lethal dose (LD 50). The oral lethal dose (LD 50) is 30 g kg^{-1} for Fe, 350 g kg^{-1} for Zn, 4.1 g kg^{-1} for Zr, 1.5 g kg^{-1} for Mn, 8.1 g kg^{-1} for Mg, 25 g for Cu kg^{-1}, indicating that they have an acceptable range of toxicity for biological applications [102]. According to statistics, since the first report of drug loading based on MOFs in 2006, many researchers have devoted themselves to this field [103-106].

Using corresponding drug delivery methods according to different therapeutic purposes, the functionally modified nano metal organic framework material particles used as a drug delivery platform can improve the therapeutic efficiency by improving the targeting ability [108].

2.2.2 Application of MOF materials in PDT research

Nano metal organic framework materials (MOFs) are a new class of porous materials in the 21st century. They have attracted much attention due to their wide applications in biosensing, drug delivery and other fields [109]. Based on the structural advantages of MOFs and the active sites of Lewis acid or base ligands, they can control the interaction and release of drugs with biological systems [110]. At the same time, the weaker coordination bonds ensure the biodegradability of MOFs. In this regard, the development of nano-metal organic framework materials containing photosensitizers to assist drugs to treat tumors is a relatively innovative research idea. Due to the adjustable structure and more selective ligands, MOFs not only have larger pore size and higher surface area, which can realize drug encapsulation but also integrate photosensitizers (PSs) into periodic arrays, such as porphyrin MOFs [111-113]. Compared with traditional PDT systems, porphyrin-MOFs have more photosensitizer loading and avoidable self-quenching behavior, so they have broad application prospects [114]. In recent years, MOFs have been widely reported as drug carriers combined with photodynamic therapy [115]. Zhou and his colleagues first reported a Zr (IV)-based targeted porphyrin MOF (PCN-224), which size can be controlled, can improve drug accumulation in cancer cells and shows significant

PDT effects [116]. Zhang's team also developed a new strategy to modify PCN-224 (TPZ@PCN@Mem) to improve its treatment efficiency in the tumor microenvironment (TME) [117]. However, it is rare that chemotherapy for nano MOFs combined with PDT achieves combined treatment [118]. In addition, there are very few reports on the targeting of tumor cells by peptide-functionalized nano MOFs [119]. Because MOFs can be surface modified [120-122], it is feasible to modify them with peptides, which can improve their tumor targeting ability [123].

2.3 Overview of self-assembly peptide

Due to the natural biocompatibility, diverse structures and dynamic self-assembly capabilities under multiple mechanisms, self-assembling peptides have shown great potential in reducing drug toxicity, improving drug targeting and improving drug delivery efficiency [124]. Peptide assembly is based on the synergistic effect of various non-covalent interactions between molecules, including hydrogen bonding, π-π stacking, electrostatic, hydrophobic and van der Waals interactions. [125-127]

One of the most important characteristics of peptide self-assembly is the strong amphiphilic nature of the molecule. The amphiphilicity caused by the hydrophobic alkyl tail allows the self-assembled nanostructures dominated by hydrophobic forces to specifically present peptide signals on the periphery, which makes it possible to design different types of bioactive epitopes on the surface of the self-assembled nanostructures. Secondly, the amino acid sequence close to the hydrophobic tail is also very important. Under certain conditions, these amino acids can form intermolecular hydrogen bonds that usually exist in the form of β-sheets, thereby further stabilizing the self-assembled structure [128]. Self-assembled CPP can improve cellular uptake through chemical modification and provide cell and subcellular specific targeting [129]. For example, Chen et al. reported an IRGD-CDD peptide can carry

Bit1 pro-apoptotic mitochondrial protein for cancer treatment that spreads within tumors [130]. Another peptide named R9-GO-203 designed by Uchida can target paclitaxel and dox to MCF-7 and ZR-75-1 cells and inhibit the MUC1-1 oncoprotein in breast cancer cell lines [131]. Davis and his team used self-assembled RAD16-II (AcN-RARADADARARADADA-CNH 2) peptide nanofibers to achieve continuous delivery of insulin-like growth factor 1 (IGF-1) to rat myocardium [132]. The NP1 polypeptide developed by our group also successfully delivered the anticancer drug ellipticine (EPT) to A549 cells [133]. Through response to stimuli, self-assembled CPP can achieve efficient drug encapsulation and release, so it is expected to become an efficient tool in the field of nanomedicine and cancer targeted therapy.

Chapter 3 Synthesis and characterization of the peptide modified nano MOF drug carrier

3.1 Materials and Methods

Materials	Materials
$ZrOCl_2 \cdot 8H2O$	Sigma
TCPP	Sigma
Benzoic acid	Millipore
DMF	Sigma
NPKMTX peptide	NanoPeptide (Qingdao) Biotechnology Ltd.
Methotrexate	Sigma
Doxorubicin	Tokyo Chemical Industry
ABDA	Sigma
PBS	Cytiva

Table 1 Materials used in Synthesis and characterization of the peptide modified nano MOF drug carrier

3.1.1 Synthesis of PCN-224 MOF

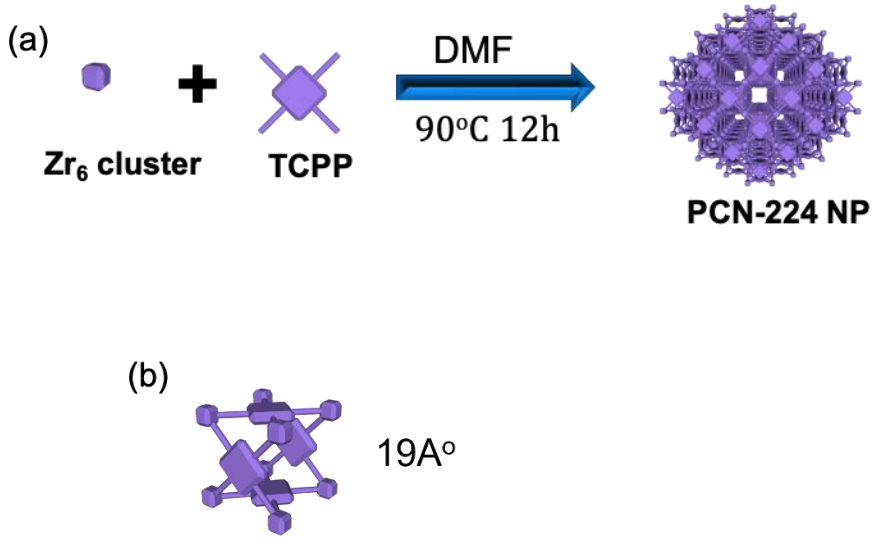

Figure 1 (a) Synthesis of PCN-224 nano MOF; (b) PCN-224 MOF unit and its size

100 mg of $ZrOCl_2 \cdot 8H_2O$ (0.31mmol), 100 mg of TCPP (0.13mmol) and 2.8 g of benzoic acid (23mmol) was weighed out and dissolved in a round bottom flask containing 100 mL DMF, and the mixture was stirred (300 rpm) at 90 ℃ for 12 h. After the reaction was complete, the PCN-224 nanoparticle pellets were washed three times with DMF and ethanol by centrifugation. The obtained PCN-224 nanoparticles were dried in vacuum, and the samples were retained for subsequent characterization and analysis.

3.1.2 Synthesis of NPKMTX peptide

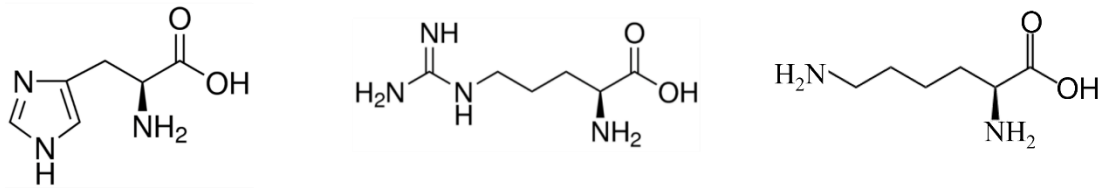

Figure 2 Amino acid residues included in NP1 and NPKMTX

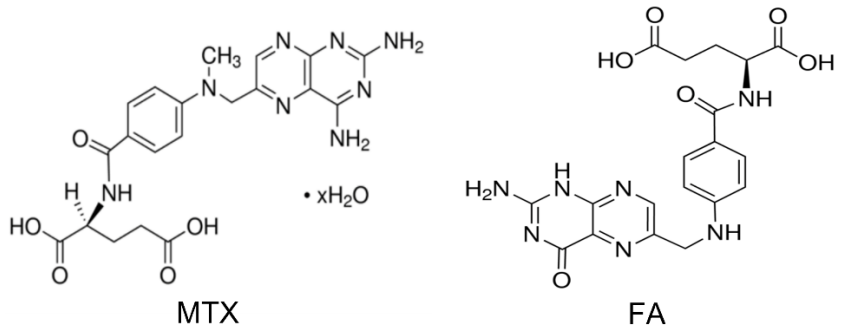

Figure 3 MTX and FA molecule structures

Name	Sequences	MW / (g/mol)
NP1	Stearyl-HHHHHHHHHHHHHHHHHRRRRRRRR-NH2	3724
NPKMTX	Stearyl-HHHHHHHHHHHHHHHHHRRRRRRRRK-MTX	4293

Table 2 NP1 and NPKMTX peptide sequences

It has been proved by earlier research of our group members that the peptide sequence NP1 (Stearyl-H16R8) developed in our group has been reported having the ability to facilitate cellular uptake and endosomal escape as well as self-assemble (disassemble) triggered by pH value in tumor microenvironment [134,135]. However, it still cannot specifically accumulate in

tumor cells through active targeting. For this reason, by introducing lysine at the end of peptide sequence to provide extra amino, a FA structural analogue MTX molecule was added to help targeting delivery and play a killing effect on cancer cells as a prodrug. The sequences and molecular weights of the designed CPPs NP1 and NPKMTX are listed in Table respectively.

3.1.3 Synthesis of Dox@PCN-NPKMTX complex

Dox@PCN-224: 2mg of PCN-224 powder was weighed and dispersed in 1ml of 0.5 mg/ml Dox solution, and the mixture was stirred (60 rpm) for 24 hours. After incubation for 1 day, the product pellets were collected by centrifugation. The supernatant was kept for further characterization to determine the drug loading efficiency. The Dox@PCN-224 (DP) sample collected was washed 3 times with MiliQ water to remove free Dox molecules not loaded in MOF particles.

Dox@PCN-224-NPKMTX: Firstly, a certain amount of NPKMTX peptide was weighed out and sonicated to completely resolve in MiliQ water and obtain a peptide stock solution with a concentration of 100μM. And then the pH value of the NPKMTX solution was adjusted to 8 and kept stable for at least 1 day. NPKMTX peptide has already self-assembled to nanostructures in this process. The Dox@PCN-224 collected in the previous step was dispersed into the peptide solution according to two mass ratios of MOF: peptide=10:1 and 10:4, and incubated for 24h with stirring. Afterwards, the product was collected by centrifugation, and the collected Dox@PCN-NPKMTX (DPN) was washed 3 times with MiliQ water. Some DP and DPN samples were dried using a freeze drier for further characterization.

3.1.4 Particle size and zeta potential

All the particle size and zeta potential data in this thesis were measured using a Zetasizer Nano ZS (Malvern Instruments, Malvern, UK) equipped with a 4 mW He-Ne laser operating at 633 nm. Disposable cuvettes (50μL, ZEN0040) with a 3 mm light path were used to collect size data of nanoparticles and the scattered light intensities were collected at an angle of 173º. Zeta potential measurements were also performed on the same machine with the manual for measurement set to zeta potential using zeta disposable cuvettes (700μl). The measurement of nanoparticle size is mainly based on the principle of dynamic light scattering (DLS), the scattering of light by particles. The Brownian motion of the particles causes fluctuations in light intensity, and tiny particles suspended in the liquid will move irregularly. The speed of Brownian motion depends on the size of the particles and the viscosity of the medium. The smaller the particle, the lower the viscosity of the medium, and the faster the Brownian motion [136,137]. When light passes through the colloid, light scattering occurs in the example, and the light signal can be detected at a certain angle. The detected signal is the result of the superposition of multiply scattered photons, so it is statistically significant. Since the laser is a monochromatic coherent laser, the laser can be used as the light source to observe the fluctuation of the scattering intensity over time. Finally, the

particle size and distribution of the sample can be calculated by the light intensity fluctuation change and the light intensity correlation function.

3.1.5 Circular dichroism spectroscopy (CDs)

Circular dichroism spectroscopy is a technique used to measure the absorption difference between left and right circularly polarized light. For asymmetric structure, chiral molecules to be specific, they would absorb left and right circularly polarized light somewhat differently which can be measured and quantified [138]. Identification of structural aspects of proteins is the most widely used application of CDs. Peptide bonds in proteins and peptides are optically active and would preferentially absorb one direction of the circularly polarized light, and their ellipticity changes the local conformation of the molecule. The peptides (100 μM) secondary structures were characterized using a J-816 Circular dichroism spectroscopy instrument. The peptide solutions (150 μL) and complex solutions were added into a 1 mm quartz cell (Hellma, Concord, Canada). Filtered MiliQ water was used for baseline measurement, and the spectra were collected from 190 nm to 260 nm with a 1 nm bandwidth at a scanning speed of 100 nm per minute.

3.1.6 Fluorescence spectrophotometer

A fluorescence spectrophotometer is a qualitative and quantitative analysis instrument for detecting substances. The principle is based on the fluorescence effect: laser irradiates atoms, the electrons in the atoms absorb energy and transition to the first excited singlet state or the second excited singlet state, but these excited states are unstable. When the electrons return from the first excited singlet state to the ground state, the energy will be released in the form of light, producing fluorescence, and generally lasts only a few nanoseconds. Through the detection of a fluorescence spectrometer, information on the excitation spectrum, emission spectrum, fluorescence intensity, and fluorescence quenching of the substance can be obtained, which is often used in biological research, pharmaceutical analysis, chemical analysis, etc. [139,140] For measuring the fluorescence, the mixture was transferred to a quartz cell and then measured by a Photon Technology International spectrophotometer (Type QM4-SE, London, Canada).

3.1.6.1 ANS fluorescence binding assay

To research the self-assembly of NPKMTX peptide, the critical aggregation concentrations (CAC) of peptide solution were determined by an ANS fluorescence assay. Different concentrations of peptides (0.625, 1.25, 2.5, 5, 10, 20, 30, 40, 60, and 100 μM)

were prepared for the measurement. 40 μL peptide solution was mixed with 40 μL ANS solution (10 μM) using vortex for 10 s. The baseline used in this experiment was ANS in Ultra-pure water. The excitation wavelength was set to 360 nm while the fluorescence spectrum was collected from 420 to 660 nm. The CAC of each peptide was determined by 475 nm ANS fluorescence intensity plotted against the concentration gradient of the peptide.

3.1.6.2 ABDA test for ROS detection

ABDA was used to determine the ability of TCPP and PCN-224 to generate active oxygen, especially $^1O_2$. ABDA molecules can react with ROS to generate internal peroxyl compounds, which leads to a decrease in ABDA fluorescence [141]. After ABDA was added, 650 nm laser (100mw/cm^2) was used to irradiate the PCN-224 (100 μg· mL^{-1}) solution and the fluorescence intensity was measured with the illumination time change (0min, 5min, 1.5h, 1d). The baseline used in this experiment was PCN-224 100 μg· mL^{-1} solution, which was also be used as the negative control, while the fluorescence intensity of the PCN-224 solution added ABDA at 0min moment was a positive control. The excitation wavelength was set to 380 nm while the fluorescence spectrum was collected from 400 to 600 nm.

3.1.6.3 Drug loading efficiency

The fluorescence of Dox is excited at 497nm, and the emission wavelength is at 595nm. The fluorescence intensity of the Doxorubicin solution with a known concentration gradient (1, 2, 5, 10, 20μg/ml) was measured to make a standard concentration curve of dox. After that, the fluorescence intensity of the sample could be calculated by measuring the supernatant obtained by centrifugation during the DP preparation process. The concentration of Doxorubicin loaded into PCN-224 MOF particles can be identified by calculating the difference between the concentration of the original Dox solution before reaction and the supernatant collected after drug loading.

3.1.6.4 Drug controlled release

The effective chemotherapy of Dox depends on the controlled drug release from the carrier. In order to research whether the Dox loaded in nano MOF particles can achieve pH-triggered release, and how the NPKMTX peptides modified outside the Dox@PCN-224 nanoparticles would influence dox release, acidic tumor microenvironment was simulated in vitro to carry out the experiments of controlled drug release from DP and DPN. The experimental device consists of a dialysis tube (2000 MWCO, Thermo Scientific), a 1.5ml centrifuge tube, and a stir bar. The dialysis tube and the 1.5ml centrifuge tube can be nested

together, and the upper and lower liquid levels can be separated by the semi-permeable membrane of the dialysis tube. The pH-adjusted PBS buffer was used to simulate the fluid environment in the body, where the neutral buffer represented the normal cell environment, and the PBS with a lower pH value represented the tumor acidic microenvironment. 110μl of each sample to be tested was added into the dialysis tubes, and the corresponding buffer was added into the centrifuge tubes below, and a stir bar was put in the buffer with stirring for 72 hours in dark. Free dox molecules released from PCN-224 nano MOF particles in the dialysis tube would slowly diffuse through the semi-permeable membrane into the buffer below. At 1h, 2h, 4h, 8h, 12h, 24h, 36h, 48h, 60h and 72h, the fluorescence intensity values of dox in PBS buffer in the centrifuge tubes were measured and recorded. These fluorescence data of each sample were used to make a drug release profile for further analysis. In this experiment, MiliQ water was used as the baseline and also as a negative control. According to the dox loading efficiency calculated by measuring the dox fluorescence intensity of the supernatant during the DP preparation process, a pure dox solution with the same total load as the DP and DPN samples in this experiment was prepared as a positive control. At the end of the experiment, the maximum fluorescence intensity value of dox in the positive control sample was recorded as 100%.

3.1.6.5 Fluorescence quenching

As we all know, (DOX) is an anticancer drug based on anthraquinone and a good electron acceptor. π-π stacking is a special spatial arrangement of aromatic compounds. It refers to a kind of weak interaction that often occurs between aromatic rings and usually exists between two relatively electron-rich and electron-deficient molecules. π-π stacking is a non-covalent interaction that is considered as important as hydrogen bonding. The face-to-edge interaction can be regarded as a weak hydrogen bond formed between a slightly electron-deficient hydrogen atom on an aromatic ring and an electron-rich π electron cloud on another aromatic ring [142]. TCPP shows ultra-high loading capacity for highly aromatic Dox molecules through strong π-π stacking interaction [143]. When PCN-224 porous structure adsorbed free dox molecules, dox was mainly loaded into MOF through π-π stacking with TCPP ligands in PCN-224 nano MOF particles. At this time, energy transfer may occur between the two adjacent fluorescent molecules TCPP and Dox, which may lead to fluorescence quenching. Analyzing the fluorescence quenching effect of TCPP and Dox, on one hand can help confirm the mechanism of Dox loading, on the other hand, it can correct the error of drug accumulation at the cellular level which was analyzed and obtained from flow cytometry fluorescence intensity measurement. Therefore, PCN-224 nano MOF

particle samples loaded with Dox were dispersed in MiliQ water as the samples to be tested, and the fluorescence intensity under the fluorescence excitation conditions of TCPP and Dox were measured respectively. In this experiment, MiliQ ultrapure water was used as the baseline, and PCN-224 solution and Dox solution of the same concentration as the DP sample were used as positive controls. The excitation wavelength of TCPP was set to 420 nm while the fluorescence spectrum was collected from 600 to 750 nm.

3.1.7 Atomic force microscopy (AFM)

Atomic Force Microscope (AFM) is an analytical instrument that can be used to study the surface structure of solid materials including insulators. One end of a micro-cantilever that is extremely sensitive to weak forces is fixed, and there is a tiny needle tip on the other end to make it lightly contact the surface of the sample. Due to the extremely weak repulsive force between the atoms at the tip of the tip and the atoms on the sample surface, the cantilever will be slightly deflected. A laser beam generated by the laser diode is focused on the back of the cantilever through a lens and then reflected the photodiode to form feedback. When scanning the sample, the micro cantilever will bend and undulate with the surface topography of the sample under the adjustment of the feedback adjustment system, and the reflected beam will also shift accordingly. Through the detected deflection amount, the position change of the micro cantilever corresponding to each point can be obtained, thereby obtaining the image information of the surface topography of the sample. An image of a sample can be captured by raster scanning across the sample surface line by line [144,145]. NPKMTX peptide self-assembled in solution with different pH values were loaded onto mica surface (50 μL), washed twice (DI water, 50μL), and air-dried for 24 h before imaging. The AFM instrument used was Dimension ICON AFM (Bruker Corporation, MA, USA), and the

Scanasyst static mode was used for imaging. The scale of the image was set to 1.5 μm to maintain the resolution ratio.

3.1.8 Scanning electron microscope (SEM)

Scanning electron microscope (SEM) is a modern research tool invented in 1965, mainly based on the interaction between electrons and matter. When a beam of high-energy incident electrons bombards the material surface, the excited area will produce secondary electrons, Auger electrons, characteristic X-rays and continuum X-rays, backscattered electrons, transmission electrons, and visible, ultraviolet, and infrared light. Electromagnetic radiation generated by the area. At the same time, electron-hole pairs, lattice vibrations (phonons), and electron oscillations (plasma) can also be generated. In principle, the interaction of electrons and substances can be used to obtain various physical and chemical properties of the measured sample itself, such as morphology, composition, crystal structure, electronic structure, internal electric or magnetic fields, and so on [146,147]. Here the secondary electron signal imaging was mainly used to observe the surface morphology of the PCN-224, DP and DPN samples.

3.1.9 Fourier transform infrared (FTIR)

Fourier transform infrared (FTIR) spectroscopy is a technique that detects chemical bonds in molecules by generating infrared absorption spectra of solid, liquid or gas samples. Infrared absorption spectroscopy is caused by molecular vibration and rotational transition. The atoms that make up chemical bonds or functional groups are constantly vibrating (or rotating), and their vibration frequency is equivalent to that of infrared light. Therefore, when the molecule is irradiated with infrared light, the chemical bonds or functional groups in the molecule can undergo vibrational absorption. Different chemical bonds or functional groups have different absorption frequencies and will be in different positions on the infrared spectrum, so that the information of chemical bonds or functional groups contained in the molecules can be obtained [148,149]. In this research, FTIR technology was mainly used to check the modification of PCN-224 nano MOF particles by NPKMTX peptides. In order to determine whether NPKMTX could be successfully modified to MOF, the FTIR spectrums of MTX, PCN-224 and PCN-224-NPKMTX (PN) samples were collected in wavenumber range of $1500cm^{-1}$~$3600cm^{-1}$. FTIR also helped to research the dynamic process and mechanism of peptide modification. PCN-224 nano MOF particles were dispersed in NPKMTX peptide solution according to the mass ratio of MOF to peptide equal to 10:4, and

the modification reaction started with stirring. PN samples with a reaction time of 0h, 2h, 6h and 12 h were collected to measure FTIR spectrums.

3.2 Results and discussion

3.2.1 Modification of NP1 peptide

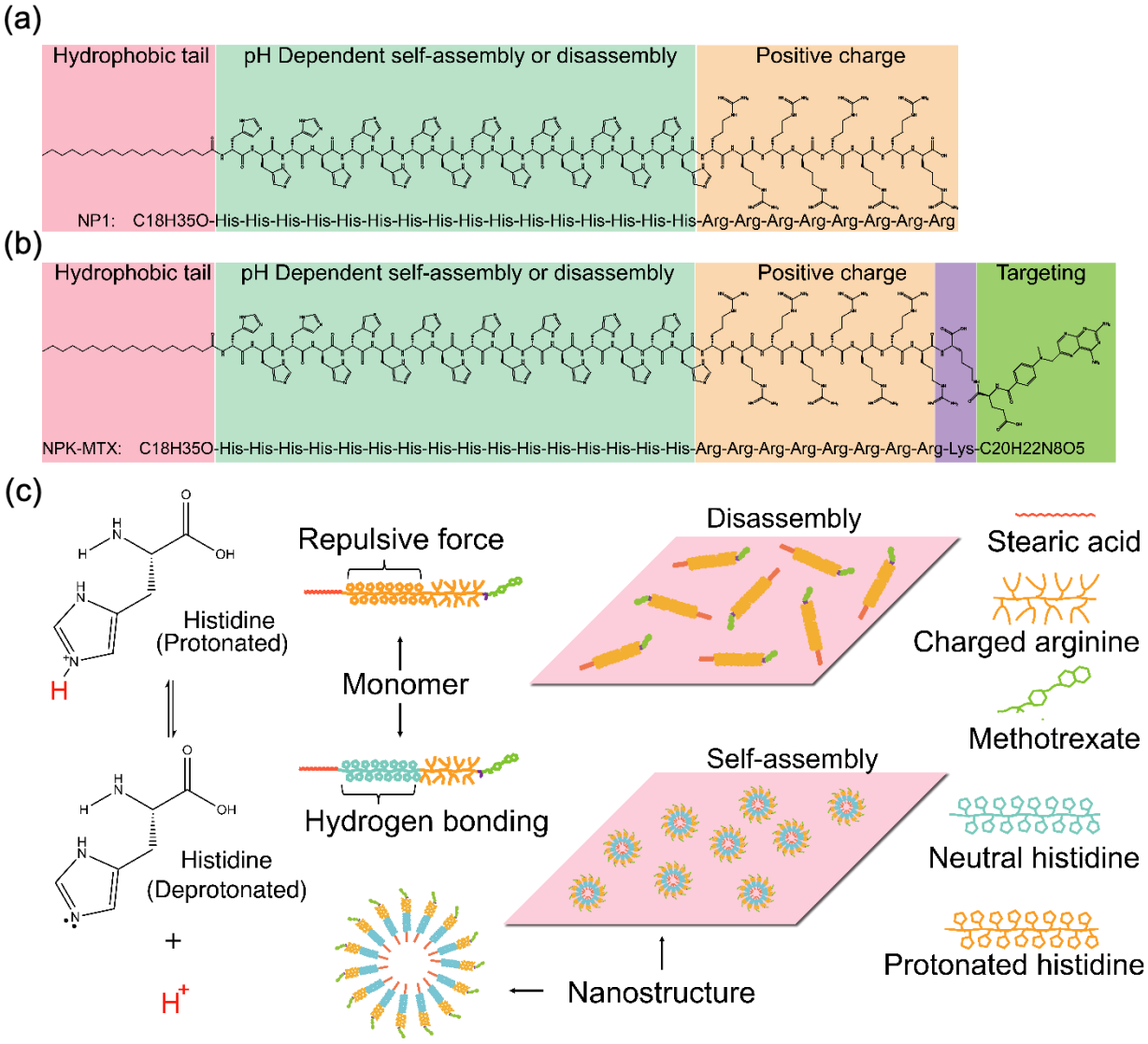

Figure 4 (a) NP1 peptide; (b) NPKMTX peptide; (c) NPKMTX self-assembly mechanism

As shown in **Figure 4**, based on the NP1 peptide reported earlier in our group, a Lysine was used to provide an extra amino group at the end of the peptide sequence. Due to steric hindrance, the carboxyl group above the gamma position in the MTX molecule reacted with the amino group on the Lysine residue to modify MTX on NP1 peptide. The formed NP1 derivative peptide, which is also a prodrug of MTX, was named by NPKMTX. Histidine is a positively charged amino acid residue, and the N on it can be protonated to show a positive charge in the H^+ ions enriched solution. In a neutral or basic liquid environment, Histidine protonation is inhibited, and hydrogen bonds are formed between adjacent histidine. The hydrophobic interaction at the end of the NPKMTX peptide plays a dominant role, which makes NPKMTX peptide self-assemble to form a micelle under the drive of hydrophobic force, exposing MTX on the outer surface. In a lower pH environment, H^+ ions will enhance the protonation of histidine. The adjacent peptide molecules in the peptide nanostructure will repel each other under the action electrostatic force because of the protonated H_{16} sequences show a great positive charge. At this time, the electrostatic force will dominate the self-assemble process, so as to achieve pH-triggered disassembly.

3.2.2 Peptide self-assembly

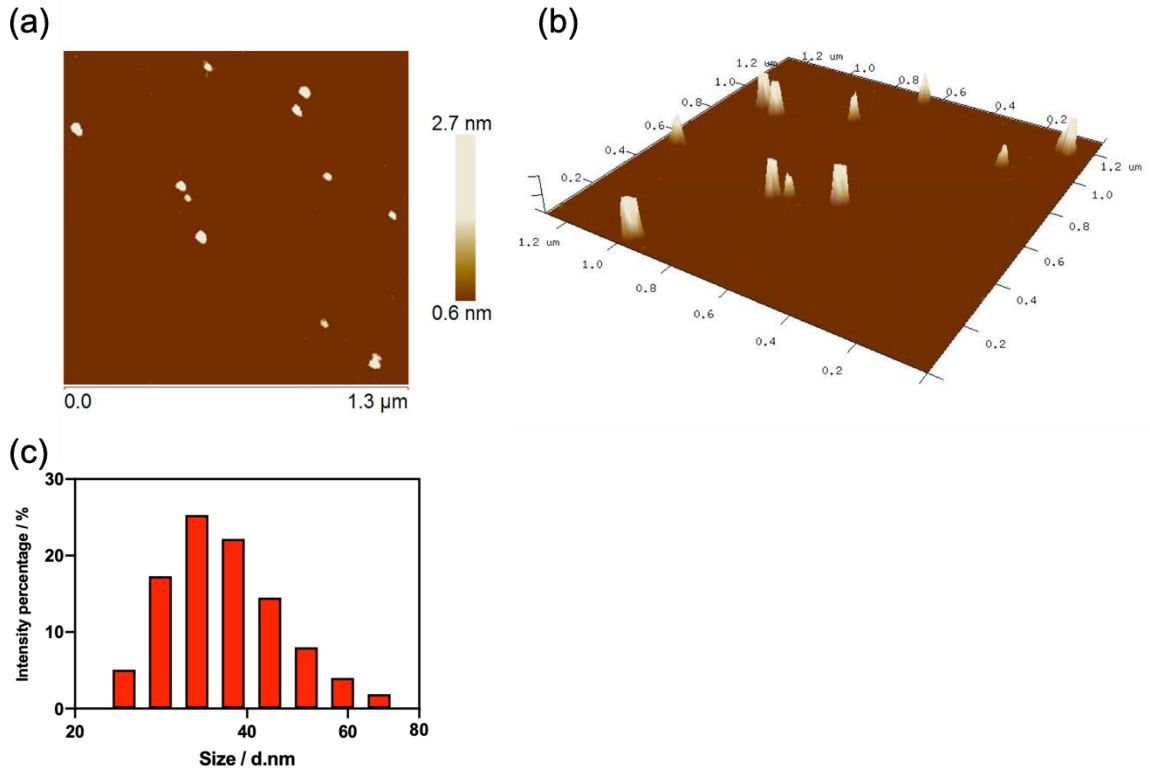

Figure 5 NPKMTX peptide self-assembly when pH=8

AFM can be used to observe the clear morphology of the peptide self-assembled nanostructures. Since the end of the alkyl chain of the NPKMTX peptide provides the relatively promising hydrophobic force, the first sample tested is the self-assembly state of NPKMTX peptide in solution with a pH value of 8. As expected, NPKMTX formed hydrophobic force driven micelle structures under alkaline conditions. As shown in **Figure 5 (a)**, it can be clearly observed that NPKMTX has formed particle structures with diameters of

about 30 nanometers. This result matched DLS data (**Figure 5 (c)**), thereby proving the self-assembly ability of the NPKMTX peptide. **Figure 5 (b)** is the three-dimensional image of **Figure 5 (a)**.

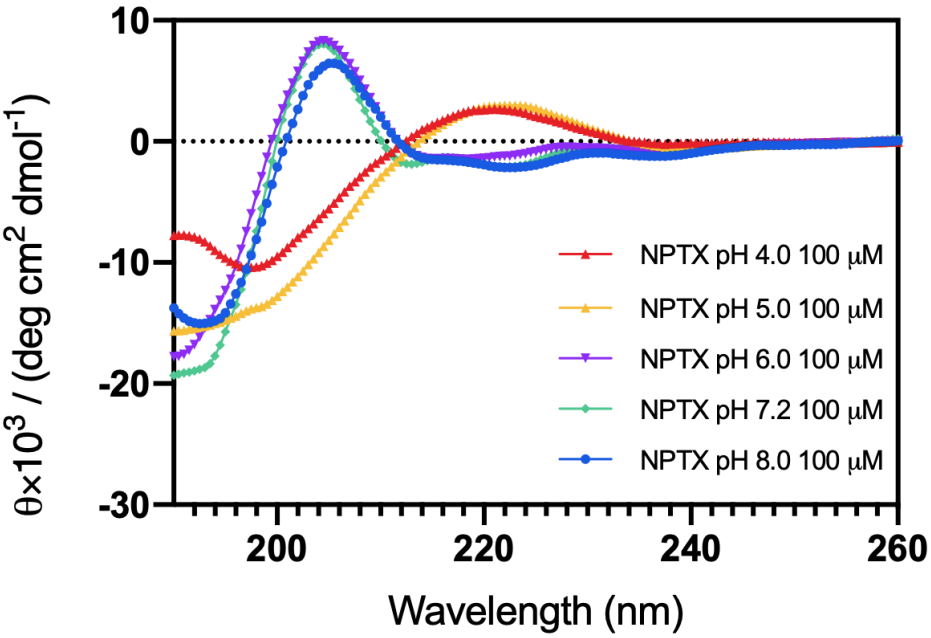

Figure 6 CDs of NPKMTX peptide with different pH values

CD is a common technical method for research of protein secondary structure. As shown in **Figure 6**, when pH= 6, 7, 8 > pKa of histidine, CDs spectrum of 100 μM NPKMTX solution shows strong characteristic peaks at 200-210 nm, indicating lots of beta-sheet structures in the three samples, which proves that the peptides in these three samples have relatively regular self-assembly structures. However, when the pH value drops to 5 and 4, which is lower than histidine's pKa, the CDs spectrum has a great change compared with

the previous samples. The characteristic peak of the beta sheet has completely disappeared, and there is an obvious broad characteristic peak of random coil at 220nm, indicating that at this time NPKMTX has been disassembled. The results of CDs verified that NPKMTX peptide still retains the self-assembly (disassembly) ability driven by Histidine protonation.

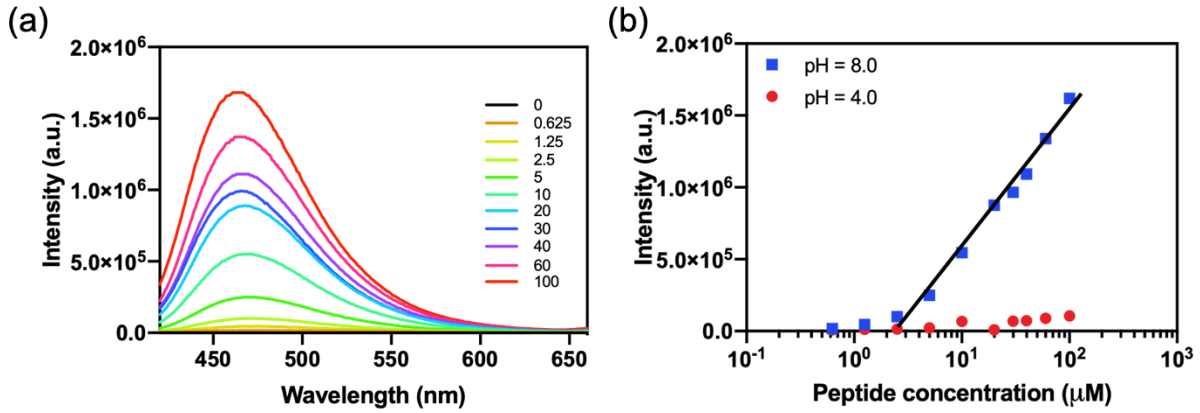

Figure 7 (a) ANS assay result of NPKMTX peptide; (b) NPKMTX critical aggregation concentration in acidic and alkaline solution

The ANS experiment is another technical method that can detect the self-assembly of peptides. ANS reagent can combine with beta sheets and be excited by 360nm light to emit fluorescence at 470 nm. In order to discover the relationship between peptide self-assembly and concentration, peptide samples with gradient concentrations and pH values of 4 and 8 were prepared, and the fluorescence intensity values were measured. Plotting the fluorescence intensity values at 470 nm into one graph, as shown in **Figure 7 (b)**, when

pH=8, Histidine residues deprotonated and ANS intensity increased from the concentration of 1.5μM, which is the critical aggregation concentration (CAC). However, the data plot of samples with pH=4 was obviously different. At this time, Histidine residues protonated and no significant signal of NPKMTX peptide self-assembly was detected even reaching the maximum concentration of 100μM. The results obtained through ANS experimental data analysis and CDs results are mutually confirmed, proving that NPKMTX can achieve sensitive self-assembly and disassembly at low concentrations (1.5μM).

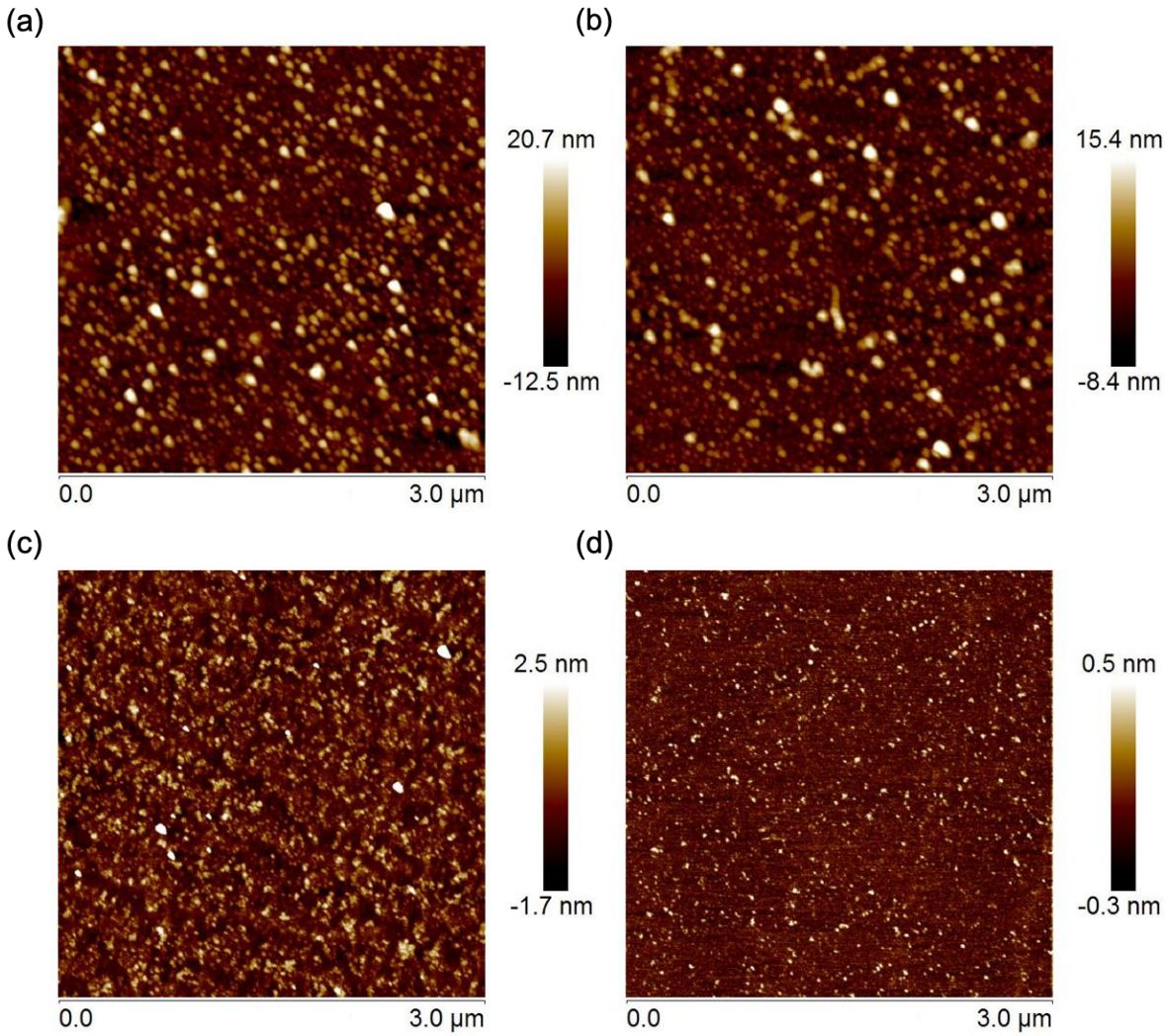

Figure 8 AFM images of NPKMTX peptide: (a) pH=7; (b) pH=6; (c) pH=5; (d) pH=4

In order to further understand the mechanism of peptide self-assembly, AFM was used to observe the structural morphology of NPKMTX nanostructures under various pH conditions to track the dynamic process of NPKMTX disassembly. Firstly, prepare a 100µM

solution of NPKMTX with pH=7, load AFM samples on mica surface, and then adjust the pH of the peptide solution to 6, 5, 4 to make AFM samples respectively. In **Figure 8**, people can clearly observe the changes in the particle structures: at the beginning, the sizes of peptide nanoparticles in the pH=7 sample were around 30-40nm, along with the decrease of pH value, the size finally became much smaller, indicating that the self-assembled morphology of the NPKMTX polypeptide will change with the change of pH values.

3.2.3 Peptide modification of MOF

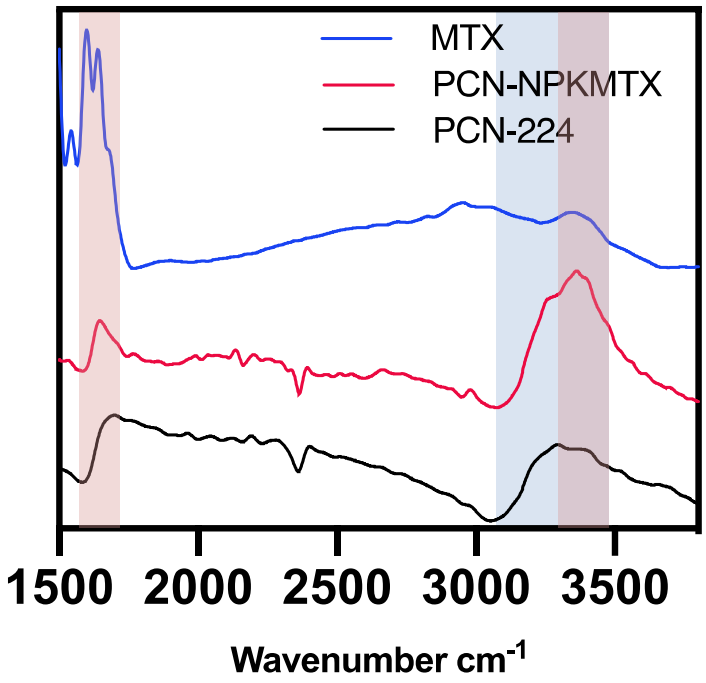

Figure 9 FTIR results of MTX, PCN-224 and PCN-NPKMTX

FTIR was used to verify whether NPKMTX peptide was successfully modified on the surface of PCN-224 MOF. The -NHR secondary amino group in TCPP has an absorption peak at a wavenumber of more than 3000 cm^{-1}, and the amino group in the MTX molecule corresponds to dual infrared absorption peaks at around 1560cm^{-1}-1640cm^{-1} and 3400cm^{-1}-3500cm^{-1}. From **Figure 9**, it can be found that PCN-NPKMTX has obvious increasing absorption peaks at 1600cm^{-1} and 3400cm^{-1}, indicating that the NPKMTSX peptide was successfully modified to the surface of MOF.

NPKMTX peptide and PCN-224 nano MOF sample were mixed to react, and the FTIR spectrums were measured at different reaction time. In **Figure 10**, a small sharp peak was observed shifting from 3298cm^{-1} to 3364cm^{-1}, or it could be described as the peak at 3298cm^{-1} disappeared while the peak at 3364cm^{-1} formed.

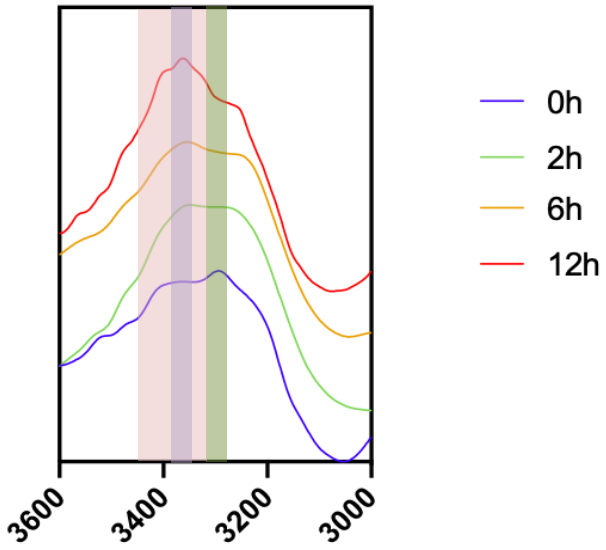

Figure 10 FTIR results of PCN-NPKMTX with different reacting time

In a solution sample, –OH's IR absorption can be observed in the range of 3200cm^{-1}~3400cm^{-1} because of hydrogen bonding. Therefore, the 3298cm^{-1} peak could be arranged as terminal –OH groups on Zr_6 clusters at the surface of PCN-224 nanoparticles. In the reaction, original terminal -OH groups on Zr_6 clusters were replaced by -COOH groups of

MTX molecules at the end of the NPKMTX peptide sequence, and some exposed uncoordinated –COOH groups were added on the surface of PCN-224-NPKMTX nanoparticles. Therefore, there were some new –OH in the PN complex. These new –OH groups as parts of –COOH groups are more stable than the original coordinated –OH groups. That means these new –OH groups need more energy to vibrate, so the peak of –OH would move to higher wavenumber (from 3298cm^{-1} to 3364cm^{-1}). At the same time, the broad pink peak indicates the addition of $–NH_2$.

3.2.4 Particle size and Morphology

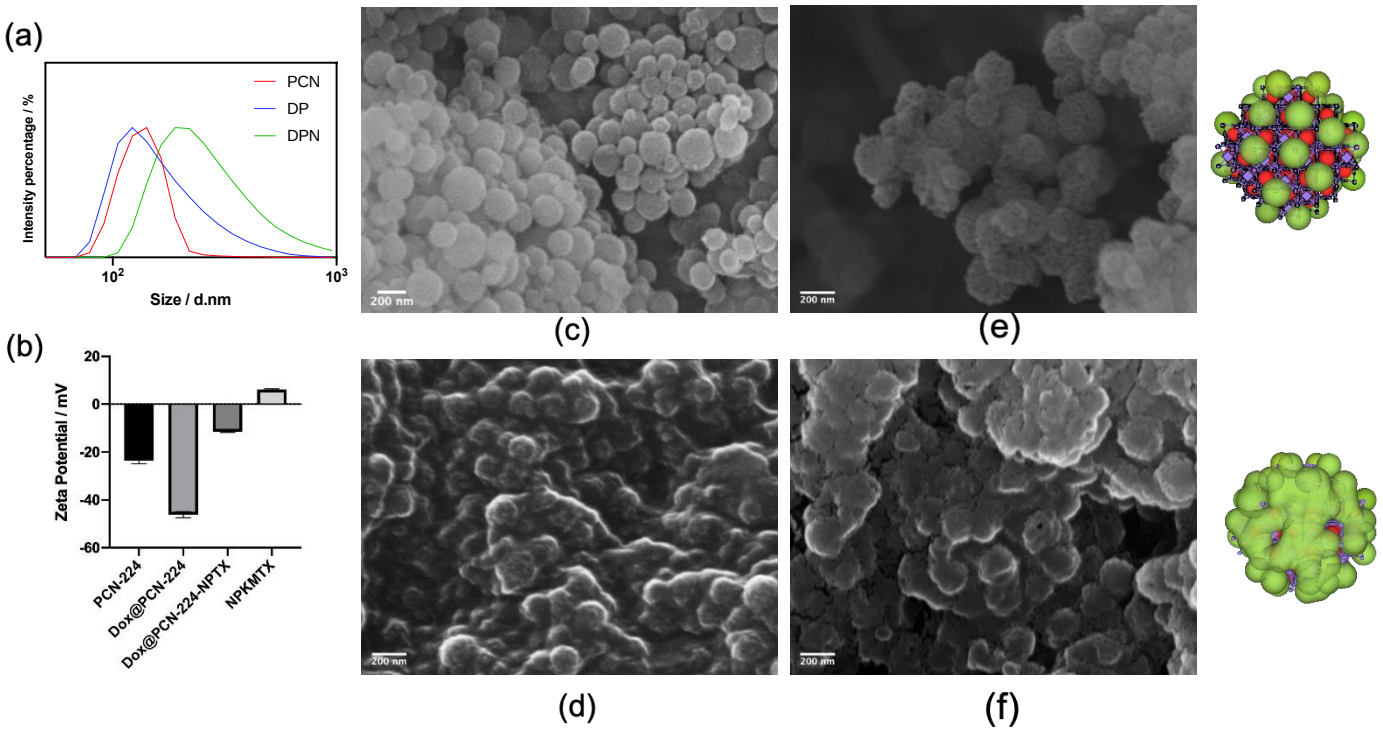

Figure 11 (a) DLS data of PCN-224, DP and DPN nanoparticles; (b) Zeta potential data of PCN-224, DP, DPN and NPKMTX nanoparticles; (c) SEM image of PCN-224 nanoparticles; (d) SEM image of DP nanoparticles; (e) SEM image and schematic diagram of DPN nanoparticles with mass ratio of MOF and peptide is 10:1; (f) SEM image and schematic diagram of DPN nanoparticles with mass ratio of MOF and peptide is 10:4

To research the size and morphology of MOF nanoparticles, PCN, DP, and DPN samples to be tested were dispersed in MiliQ water. The sizes were measured by DLS. As shown in **Figure 11 (a)**, the size distribution of PCN-224 nano MOF particles almost didn't change before and after loading dox. After modifying NPKMTX, the size distribution peak shifted to the right indicating the growth of MOF particle size. DLS results help prove that dox was loaded in the porous inner space inside PCN-224 nanoparticles instead of simply

being absorbed on the surface. The growth in size of DPN particles could be explained as the NPKMTX peptide forming a layer coating outside of PCN-224 nanoparticles. In **Figure 11 (b)**, Zeta potential analysis shows that PCN-224 nanoparticle is negatively charged when dispersed in water. This may be because the coordination sites on the Zr_6 cluster exposed on the periphery of PCN-224 were occupied by hydroxyl groups. After loading dox which is also negatively charged, the total zeta potential decreased. After modifying the positively charged peptide, the overall potential increased partly. This phenomenon also reflected the successful loading of dox and the modification by NPKMTX peptide.

In order to visually observe the modification of MOF, SEM was used for microscopic imaging. In **Figures 11 (c)**, **(d)**, **(e)** and **(f)**, it can be found that PCN-224 nano MOF particles are spherical with a smooth surface. After loading Dox, there were adhesions between adjacent MOF particles in the DP sample, this may be caused by the free overflow of Dox during the drying process of the sample. In the DPN sample with a mass ratio of MOF and NPKMTX of 10:1, it can be clearly observed that the surface of the spherical MOF particles was covered by a layer of granular structures, which is the self-assembled peptide. In the DPN sample with a mass ratio of MOF and NPKMTX of 10:4, due to the increase in the amount of peptide, the peptide outside the MOF arranged more tightly almost with no gaps,

thereby sealing the porous nano MOF structures much more perfectly. Therefore, this mass ratio of 10:4 was used as the protocol for the synthesis of DPN.

3.2.5 ROS generation

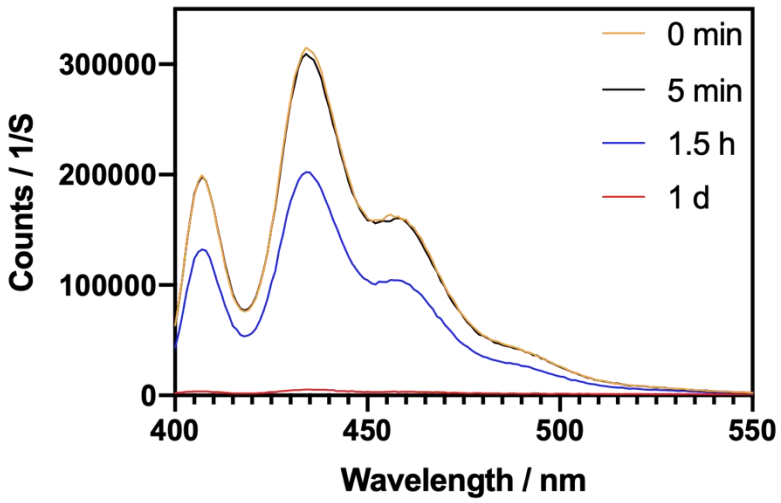

Figure 12 ABDA results

TCPP is a photosensitizer that can produce reactive oxygen species under specific wavelength laser irradiation. ABDA is often used to detect reactive oxygen species. ABDA can bind to ROS, which causes the fluorescence intensity of the ABDA reagent to decrease accordingly. As shown in **Figure 12**, at 0 min, there is a sharp fluorescence peak at a wavelength of 435 nm. After 5 min, the fluorescence decreased 6000 counts s^{-1}, indicating that ROS was formed.

3.2.6 Drug loading and release

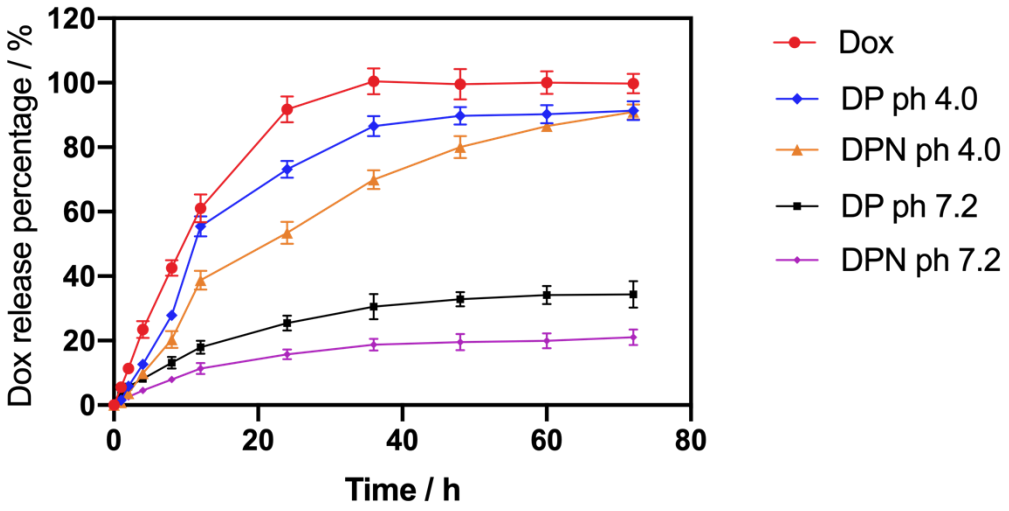

Figure 13 Dox release profile

Without a sealing layer, some dox would escape from nano MOF particles randomly. Therefore, NPKMTX peptide with self-assembly function can not only target the folate receptor but also encapsulate dox loaded inside PCN-224. Under normal pH conditions, the nanostructures composed of NPKMTX are tightly wrapped outside the pores of the MOF, preventing the escape loss of Dox during the delivery process. In the cancer cell microenvironment with a lower pH value, NPKMTX peptide will disassemble driven by Histidine protonation, which will loosen the peptide coating layer and expose the porous channels of the inside PCN-224 nano MOF particles. At the same time, low pH weakens the π-π stacking effect between dox and TCPP and dox is released. It is worth mentioning that

because the disassembly is a slow process, the drugs encapsulated in the MOF can be released slowly, prolonging the time for the entire DPN system to exert its effects.

Figure 13 shows the release curve of the drug-loaded delivery system. The dox solution with corresponding concentration of DP and DPN sample was used as a positive control. It can be seen from **Figure 13** that at 36h, the release of the dox solution as a positive control had reached the maximum release amount, which was taken as 100 %. When pH=4, the DP sample had reached the maximum release amount in about 40h, which was about 90% of the initial load amount. At normal pH (7.2), part of dox loaded in DP would escape randomly, and it stabilized at 36h, and finally about 30% of dox was released. This result verified that dox was loaded in PCN-224 by π-π stacking with TCPP linker, and low pH values can indeed regulate the release of dox. From the profile of drug release of DPN sample in lower pH environment, it could be found that the release rate of DPN was lower than that of DP sample, and it did not reach the highest release until 72h, indicating that the NPKMTX coating layer was slowly disassembled under pH adjustment. The drug release time was nearly doubled, and the final total drug release amount was not affected. It is worth mentioning that in a normal pH environment, DPN also showed a very low release ratio

(about 17%), which was nearly half less than that of the uncoated DP. It can be seen that the DPN drug-loaded delivery system can achieve good pH-controlled release.

3.3 Conclusions

By taking into consideration the peptide assembly and the ability to target folate receptors, NP1 was rationally modified with MTX at the end of the original sequence in order to improve the targeting function while maintaining the self-assembly ability. According to the ability of nanoparticles with different sizes to enter cells, spherical PCN-224 MOF nanoparticles with appropriate size were synthesized. After ABDA testing, PCN-224 MOF was proved can generate ROS under specific light irradiation and then have PDT capability. Through π-π stacking, dox was loaded into PCN-224 MOF nanoparticles, and then the NPK-MTX peptide was also modified on the surface of the MOF particles through coordination bonding to encapsulate drugs and provide targeting function, thus successfully constructing a DPN drug delivery system. Due to the hydrophobic effect of the stearic acid part of the NPKMTX peptide and the self-assembly ability of deprotonated histidine, when the pH value decreases, the NPKMTX peptide modification layer coated on the surface of the PCN-224 MOF nanoparticles will disassemble and decompose into random coils, thereby exposing the internal pores of PCN-224. In the acidic microenvironment of tumor cells, a lower pH value will weaken the π-π stacking effect between Dox and TCPP and then trigger drug release.

Chapter 4 In vitro test

4.1 Materials and methods

Materials	Materials
Hela Cell line	ATCC
A549 Cell line	ATCC
HEK293 Cell line	ATCC
F-12K medium	Thermo Fisher Scientific
DMEM medium	Cytiva
FBS	Sigma
Trypsin	Thermo Fisher Scientific
CCK-8	Dojindo Molecular Technologies
PFA	Sigma
Folic Acid	Sigma

Table 3 Materials used in cell experiments

4.1.1 Cell culture

A549 (human lung cancer cell line), Hela (human cervical cancer cell line) and HEK293 (human embryonic kidney cell line) cell lines were purchased from American Type Culture Collection. A549 cells were cultured in F-12K medium supplemented with 10% fetal bovine serum (FBS). Cells were incubated at 37ºC in a humidified atmosphere containing 5% CO_2. The culture medium was removed and replaced every two days. DMEM medium with 10% PBS was used for Hela and HEK293 cell culture. When the cells are cultured to a certain amount, the required cells were taken out of the cell culture flask 1 day before the experiment. Trypsin was used to make the cells fall off from the culture flask. When most of the cells fall off, serum-containing medium as much as 3 times the volume of trypsin was added to the cell suspension to stop the digestion. The cell suspension was centrifuged at 1500 rpm for 5 minutes and finally resuspend in the corresponding medium with a certain concentration, and then cells were seeded according to the experimental requirements.

4.1.2 Cytotoxicity

To determine the cytotoxicity of the materials dosed on different cells, cell counting kit-8 (CCK-8) assay was used to measure the cell viability. CCK8 will be reduced by dehydrogenase in the mitochondria to a highly water-soluble orange-yellow formazan product due to the electron carrier 1-Methoxy PMS [150]. The color depth is proportional to the number of living cells for the same cell line. In the cytotoxicity experiment, a lighter color indicates fewer living cells, thereby the material dosed with is more cytotoxic. Therefore, CCK-8 assay can be used to directly analyze cell proliferation and toxicity.

A FLUOstar OPTIMA microplate reader was used to measure the CCK8 absorbance at 570 nm. The absorbance data will be analyzed and expressed as the ratio of the cells treated with the carriers over the non-treated cells (negative control).

4.1.2.1 Biocompatibility of PCN-224

The biocompatibility of PCN-224 to A549 and Hela cells was tested by CCK-8 assay. A549 and Hela cells (8,000 cells/well) were seeded in 96-well cell culture plates in the corresponding medium with 10% FBS. After 24-hour incubation, the confluence of cells

reached over 50%. Cells were dosed with PCN-224 nano MOF particles with various concentrations (from 1μg/ml to 80μg/ml) and incubated at 37ºC in a humidified atmosphere containing 5% CO_2 for 24 hours. After the incubation, the sample-containing medium was removed, and cells were treated with diluted Cell Counting Kit-8 (CCK8) reagent (11 times dilution) for around 20 minutes or until the absorbance reading of non-treated cells reached 0.7 or higher.

4.1.2.2 Photodynamic therapy leading apoptosis

Hela cell line was selected as the model to verify the PDT effect of PCN-224 nano MOF particles. Cell processing and administration are similar to the previous part. After dosing PCN-224 for 12 hours, the cells were irradiated with a laser with wavelength of 650 nm for 20 minutes, and the CCK-8 experiment was carried out after continuing the incubation for 12 hours.

4.1.2.3 Chemotherapy leading apoptosis

A549 and Hela cells (8,000 cells/well) were seeded in 96-well cell culture plates in the corresponding medium with 10% FBS and incubated for 24 hours until the confluence of cells reached over 50%. Cells were dosed with NPKMTX peptide, PN, DP and DPN with

corresponding various concentrations and incubated at 37ºC in a humidified atmosphere containing 5% CO_2 for 24 hours. The data collection and analysis methods are consistent with the description above.

4.1.3 Fluorescence-Activated Cell Sorting (FACS)

Flow cytometry is a high-tech technology that uses a flow cytometer to simultaneously perform multi-parameter, rapid quantitative analysis and sorting of cells or biological particles in a fast-linear flow state. Firstly, the cells or particles to be tested are made into a single cell suspension, which is stained with specific fluorescent dye-labeled antibodies and enters the flow chamber under constant gas pressure. And then, cells or particles to be tested are arranged in a single row with the coating of the sheath fluid and pass through the detection area in turn. Laser usually is used as the light source of a flow cytometer. The focused and shaped beam is irradiated vertically on the sample stream, and the fluorescent dyes on the cells or particles are excited to generate scattered light and excite fluorescence. After these fluorescent signals are detected, they are converted into digital signals that can be recognized by the software. The data results can be used to analyze the measured cell membrane surface antigen intensity or intracellular substance concentration [151-154]. Cellular uptake of DP and DPN nanoparticles was studied with fluorescence-activated cell sorting (FACS) using flow cytometry (BD Biosciences, BD FACS Vantage SE Cell Sorter, USA). A549, Hela and HEK293 cells were seeded at a density of 100,000 cells/well in 24-well plates and incubated in a 5% CO_2 incubator at 37°C. 24 hours later, the

confluence of cells reached 80%, and then the cells were dosed with DP and DPN nanoparticles (PCN-224 40μg/ml). Cells none-treated and treated with Dox or TCPP alone were also included in the experiments as controls. The dosed cells were incubated for 3 hours at 37°C and then processed for FACS. In detail, the cells were rinsed with Opti-MEM containing heparin for 20 minutes in the incubator at 37°C for three times followed by PBS washes twice with occasional shaking. Thereafter, the cells were detached with 0.25% trypsin/EDTA for 5 minutes and fixed with 2% paraformaldehyde (PFA) in PBS and then collected in tubes, wrapped in tinfoil and stored at 4ºC prior to FACS. Data were analyzed by Flowjo software afterwards.

4.1.4 Confocal laser scanning microscope (CLSM)

Confocal laser scanning microscope (CLSM) is one of the most important developments of modern biomedical imaging instruments. It is based on fluorescence microscope imaging with a laser scanning device that uses ultraviolet light or visible light to excite fluorescence detection. The fluorescence signal is processed by a computer to obtain a fluorescent image of the fine structure inside the cell or tissue. This technology has been widely used in the fields of cell biology, physiology, pathology, anatomy, embryology, immunology and neurobiology. It has great advantages for qualitative, quantitative, timing and positioning research on biological samples and become a new generation of powerful research tools in these fields [155-157]. In this research, cellular fluorescence imaging was acquired with a Zeiss LSM 700 confocal microscope.

4.1.4.1 Drug distribution in cells

In order to further research the process of functionalized MOF nanoparticles entering and taking effect in cancer cells, confocal laser scan microscope (CLSM) was used to perform fluorescence tracer imaging on A549 and Hela cells. The experiment process is kind of similar to the FACS experiments except for detaching. Two kinds of cells were seeded at a density of 15,000 cells/well in 6 well plates with a glass bottom and they were used for

CLSM imaging with the corresponding medium. After incubation in a 5% CO_2 incubator at 37°C for 24h, cells grew adherently at a density suitable for observation. And then the cells were dosed with DP and DPN nanoparticles (PCN-224 40μg/ml), none treated cells were also included in this experiment as negative controls. The dosed cells were incubated for 3 hours at 37°C and then processed for CLSM. In detail, the cells were rinsed with PBS washes twice to remove the residual nanoparticles in the medium. Thereafter, the cells were fixed with 4% paraformaldehyde (PFA) in PBS.

4.1.4.2 Competition assay

In order to confirm the active targeting function of NPKMTX peptide modified PCN-224 nano MOF particles on folate receptor, a competition assay was performed using DP and DPN in the presence of excess free folic acid (FA) as a competing ligand for folate receptor. The experiment selected folate receptor negative cells A549 and folate receptor positive cells Hela for control. The cell seeding plate and the nanoparticle dosing method are the same as above besides adding excess amount of FA (1mM) in the folic acid competition control group at the same time. After incubation and fixation, the cells were used to observe the intracellular drug fluorescence intensity distribution through CLSM imaging.

4.2 Results and discussion

4.2.1 Cytotoxicity

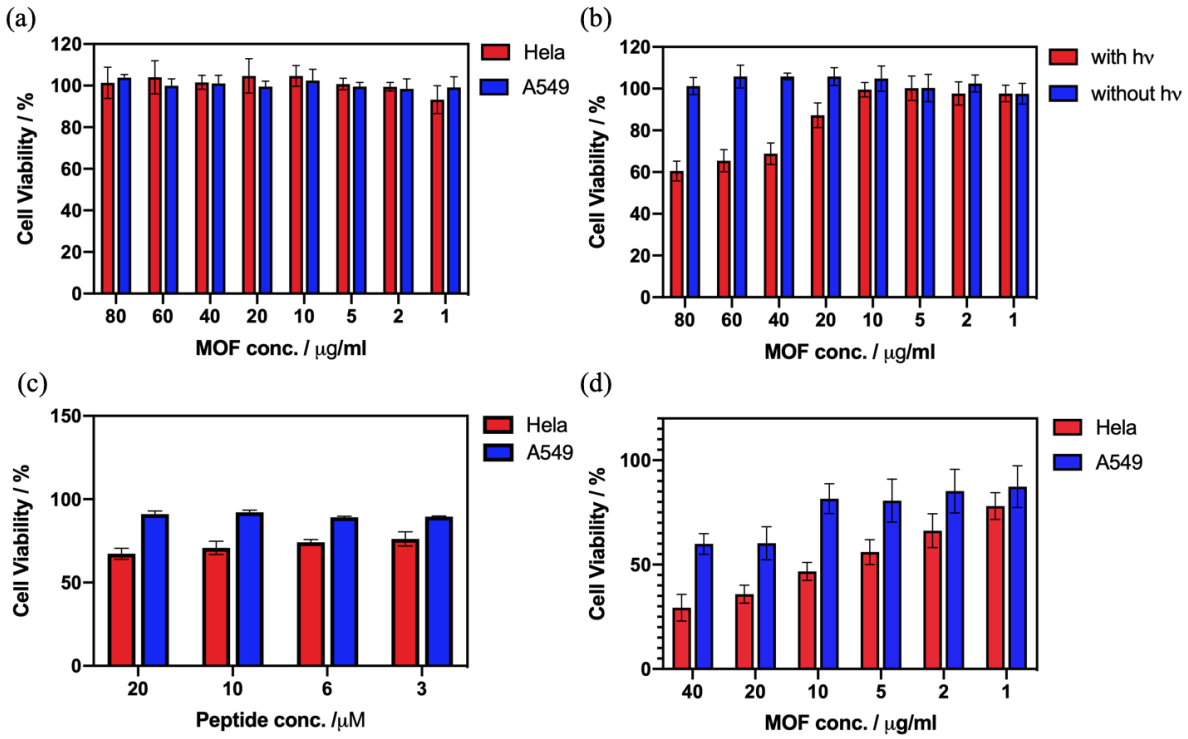

Figure 14 Cytotoxicity results of (a) PCN-224, (b)PCN-224 PDT, (c) NPKMTX peptide and (d) PCN-224-NPKMTX

As a drug delivery vehicle, the carrier material must be safe and biodegradable in vivo. MOF coordination composition is easy to be degraded and metabolized, and it has been proved to be relatively safe. As shown in **Figure 14 (a)**, two cancer cell lines, A549 and Hela, were selected for cytotoxicity testing, and the results proved that PCN-224 MOF itself

has no damage to cells. In order to verify the effect of PDT, the Hela cell line was selected as a model. The dose amount ranged from 1 μg/ml to 80μg/ml, and each well was irradiated with a 650nm laser for 20 minutes. In **Figure 14 (b)**, it was found that in samples with concentration of 20-80μg/ml, PCN-224 MOF exposed to light showed a lethality proportional to the dose. However, the dose with a concentration below 10 μg/ml did not show the lethality, which may be due to the reductive GSH over-expressed by Hela cancer cells consumed the small amount of ROS produced by low-concentration TCPP. In order to research the cytotoxicity of NPKMTX peptide to cancer cells, two cell lines A549 and Hela were selected here and dosed with NPKMTX peptide with a concentration of 3-20 μg/ml. From **Figure 14 (c)**, people can find that NPKMTX basically has no lethality against A549 cell line, but it has certain lethality against Hela cell line. This is because there are overexpressed folate receptors on the surface of Hela cells while A549 is folate receptor negative cell. During the dosing process, the MTX molecule at the end of the NPKMTX peptide sequence can be specifically recognized by the folate receptors of Hela cells, thereby making NPKMTX peptide enter Hela cells more easily and release MTX to exert chemotherapy effect.

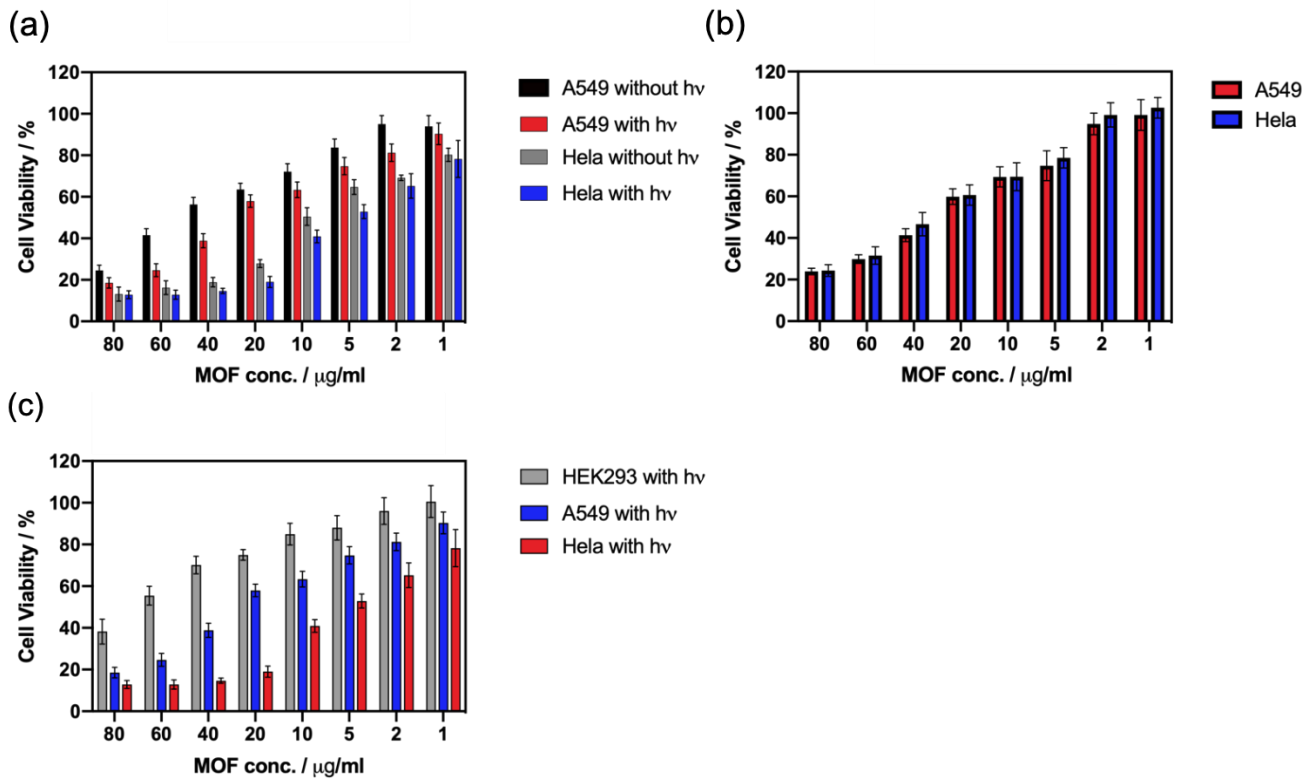

Figure 15 Cytotoxicity results of (a) DPN with or without irradiation, (b) DP and (c) DPN with irradiation on 3 cell lines

In order to further know whether NPKMTX modification can help PCN-224 MOF nanoparticles selectively enter folate receptor positive cells, NPKMTX modified unloaded PCN-224 MOF nanoparticles (PN) were prepared. A549 and Hela cell lines were used for comparison. The dosage was based on the MOF concentration, from 1μg/ml to 40μg/ml. The results were analyzed and plotted in **Figure 14 (d)**. In the results of the Hela cell line, it can

be clearly seen that PCN-NPKMTX showed a lethality proportional to the concentration of PN, and the half lethal dose was about 10μg/ml. In the results of the A549 cell line, although PCN-NPKMTX can also be observed to have a certain lethality, the estimating half-lethal dose was about 50μg/ml, which is a huge difference from the Hela group. This result can also indicate that the modification of PCN-224 MOF nanoparticles by NPKMTX peptide can help the nanoparticles to enter folate receptor-positive cancer cells more easily. From the comparison of **Figures 14 (a)**, **(c)**, and **(d)**, we found that PCN-224, which is non-toxic by itself, showed a certain lethality after modification by the non-toxic NPKMTX peptide against A549 cells. This is because the size of modified MOF nanoparticles was around 200 nanometers, and nanoparticles with this size can enter cells more easily, so the NPKMTX peptide on the surface entered A549 cells along with PCN-224 nanoparticles through passive targeting and released MTX molecules and exerted chemotherapy effect.

To identify the ability of PCN-224 MOF nanoparticles as drug carriers to enter cancer cells and conduct their chemotherapy effect, we used Dox@PCN-224 nanoparticles (DP) which were loaded with dox but without peptide modification for cytotoxicity tests, A549 and Hela cell lines were still used as control groups of cells with negative and positive folate receptors. As shown in **Figure 15 (b)**, the lethality of Dox@PCN-224 was almost the same

against the two cell lines, which indicated that DP could pass through the nanoparticle and play a role on both cancer cell lines. Because DP nanoparticle passive targeting was not selective on two types of cells, the low pH environment in both A549 and Hela cancer cells can control the release of dox, the killing effect on the folate receptor-negative and positive cells should be basically the same.

In order to research whether MOF nanoparticles loaded with dox and modified with NPKMTX peptide (DPN) still have PDT efficacy, we also used A549 and Hela cell lines as models, and the doses ranged from 1μg/ml to 80μg/ml with and without light interaction as control groups. As shown in **Figure 15 (a)**, DPN showed greater lethality with light irradiation than the sample without light in both A549 and Hela cell results.

Finally, to verify whether the entire NPKMTX-modified Dox-loaded PCN-224 MOF nanoparticles (DPN) have selective lethality against folate receptor-positive cancer cells at the cellular level, HEK293, A549 and Hela cell lines were selected for cytotoxicity experiment. HEK293 is a normal cell model with folate receptor (FR) negative and the other two cancer cell lines served as a control group for each other. As shown in **Figure 15 (c)**, DPN dosing combined with irradiation showed huge differences in lethality against the three cell lines. Among the results, the half lethal dose of Hela cells was 5μg/ml, that of A549 cells

was about 30μg/ml, and that of HEK293 cells was about 50μg/ml. Firstly, the NPKMTX peptide molecules modified outside DPN were specifically recognized by the FRs overexpressed on the surface of Hela cells, so that DPN could enter Hela cells more easily. The acidic internal environment of cancer cells triggered the disassembly of NPKMTX peptide and the release of Dox, and the NPKMTX peptide acting as prodrug was degraded in the lysosome to release MTX, along with the ROS generated by TCPP under irradiation, causing the massive killing of Hela cells. In contrast to the Hela cell line, although A549 is also a cancer cell line as Hela, and the internal acidic environment can also control the release of drugs, A549 cells do not overexpress folate receptors, and the DPN drug delivery system can only accumulate in A549 cells through the passive targeting effect of nanoparticles. Therefore, the DPN particles entering A549 cells were much fewer than that of Hela cells, thus showing weaker lethality. HEK293 is a normal cell negative for folate receptors. DPN nanoparticles can also enter the HEK293 cells, but the internal environment of HEK293 cannot trigger the disassembly of NPKMTX peptide and the release of dox. Only the ROS produced by TCPP in PCN-224 MOF with light irradiation, the randomly escaped Dox and a small amount of MTX generated by the degradation of NPKMTX peptides can kill cells, so the total lethality was greatly reduced compared to Hela cells. In the actual

application process of photodynamic therapy, non-tumor sites should be avoided receiving specific wavelength laser irradiation. At this time, the lethality of the DPN drug-loaded delivery system on normal cells will be further reduced, so that the half lethal dose of HEK293 can reach about 70 μg/ ml. Therefore, it can be proved that at the cellular level, the DPN drug delivery system can selectively kill a large number of tumor cells that express positive folate receptors, while greatly reducing the side effects on normal tissue cells.

4.2.2 Fluorescence-Activated Cell Sorting (FACS)

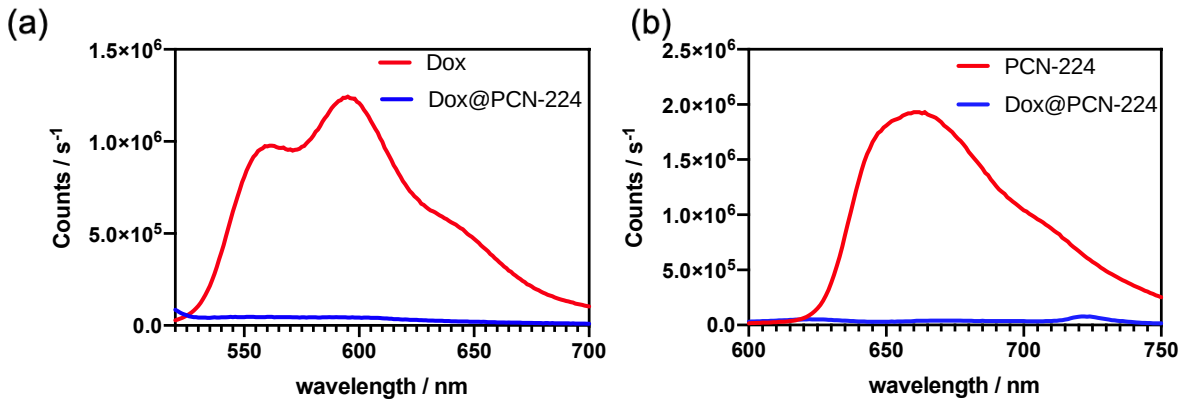

Figure 16 Fluorescence quenching of (a) Dox and (b) TCPP

Both Dox and TCPP have fluorescent properties, so FACS technology can detect two fluorescent signals in the three types of cells HEK293, A549 and Hela respectively, so as to obtain the cellular uptake data of DPN of the three cell lines. In this experiment, the targeting function of NPKMTX peptide modification was determined through comparing the cellular uptake of DP and DPN nanoparticles. Untreated cells were used as a negative control and Dox and TCPP solution treated cells were used as the positive control in the result of two fluorescence channels. As shown in **Figure 16**, dox and TCPP with the same concentration of each included in DPN were used as positive controls, and the fluorescence signals of Dox and TCPP cannot be detected in the DPN sample. This may be due to the fact that the fluorophores Dox and TCPP were too close and produced a fluorescence quenching effect.

This result helps to prove that the mechanism of PCN-224 loading doxorubicin is that Dox and TCPP in PCN-224 MOF nanoparticles are combined by π-π stacking. Therefore, the fluorescent signals detected in the FACS results were dox released from the DPN entered the cell and TCPP that no longer carries Dox.

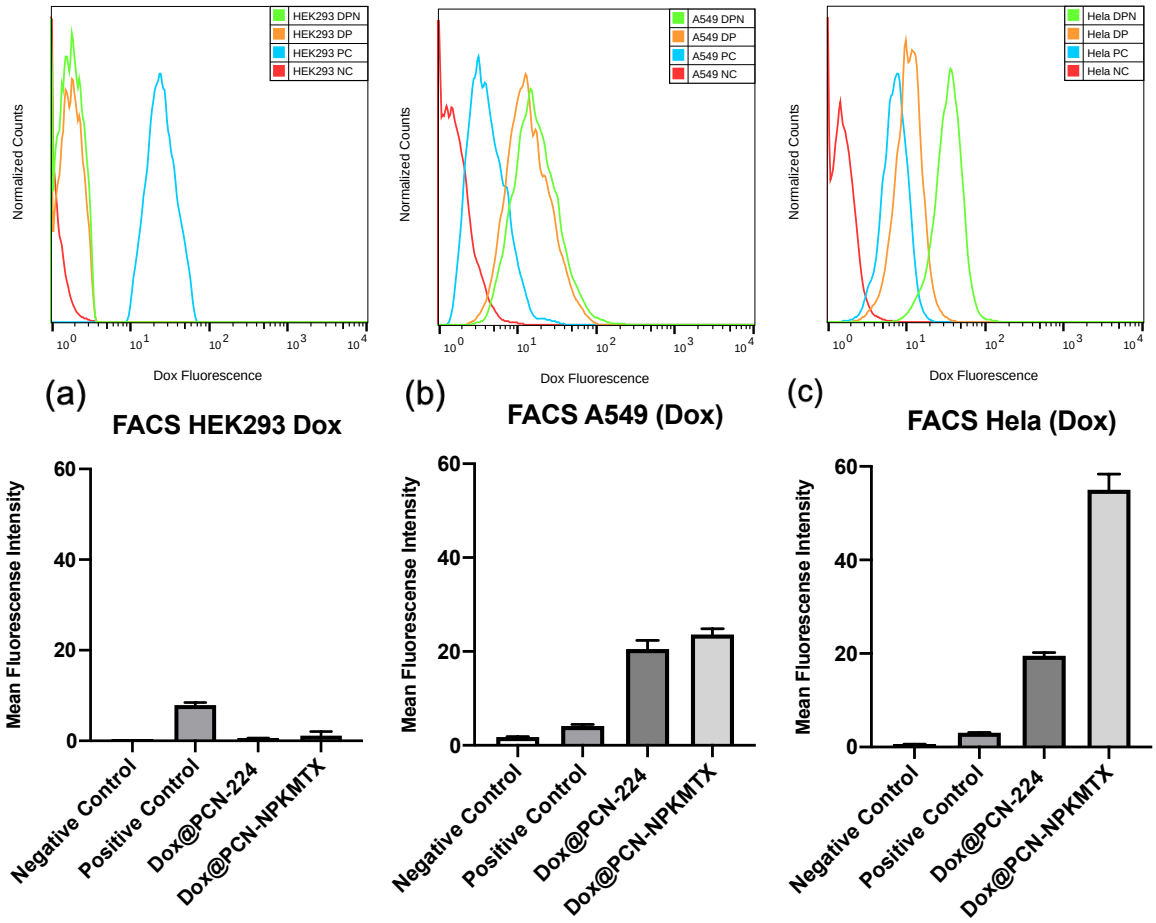

Figure 17 Dox fluorescence channel FACS data of treated (a) HEK293 cells, (b) A549 Cells and (c) Hela cells

As shown in the FACS results of the Doxorubicin fluorescence channel (**Figure 17 (a)**), in the HEK293 sample, only the positive control group treated with pure Dox solution showed an obvious Dox fluorescence signal. Compared with the Dox positive control, results of DP and DPN treated cell samples only showed a very small amount of Dox fluorescence signal, indicating that neither DP nor DPN released a large amount of Dox in HEK293 cells. As shown in **Figure 17 (b)**, the Dox fluorescence signal intensities of the DP and DPN groups in the A549 cell samples were basically the same with no significant difference, and they were both significantly stronger than that of the Dox-treated positive control group. This is because Dox loaded in PCN-224 nanoparticles is easier to enter cancer cells than free Dox small molecules and can be released in an acidic environment. Since A549 cells do not have the FRs which can specifically recognize NPKMTX peptide, there was no significant difference in the amount of DP and DPN nanoparticles entering A549 cells, so the fluorescence intensities of the two were nearly equivalent. In the Hela cell sample results (**Figure 17 (c)**), it can be found that not only the Dox fluorescence signals of DP and DPN were stronger than that of the Dox control group, but also the Dox fluorescence of the DPN group was much stronger than that of the DP group. The numerical analysis of the fluorescence intensity of the DPN group was about 2.5 times of DP group. This result proved

that NPKMTX peptide can help PCN-224 nano drug carriers to enter Hela cells with folate receptor overexpression.

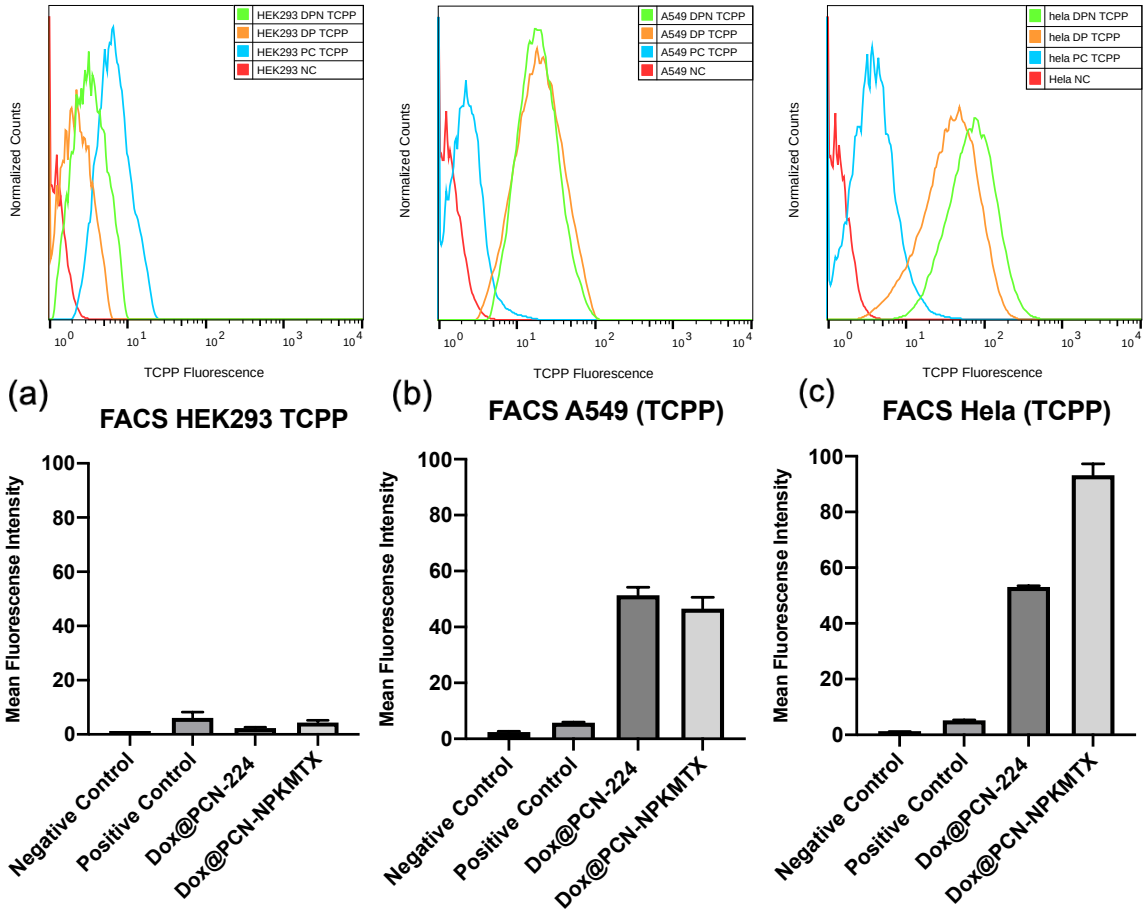

Figure 18 TCPP fluorescence channel FACS data of treated (a) HEK293 cells, (b) A549 Cells and (c) Hela cells

In order to make the research more rigorous, the FACS data of the TCPP fluorescence channel was also collected (**Figure 18**). It was very similar to the FACS data of Dox. In the HEK293 cell samples (**Figure 18 (a)**), DP and DPN had only very weak fluorescence signals. In the A549 cell samples (**Figure 18 (b)**), DP and DPN have similar fluorescence intensities and were stronger than the fluorescence signal of the TCPP control group. In the Hela samples (**Figure 18 (c)**), the fluorescence signal strength of the DPN group was approximately twice of the DP group. The FACS results of the two fluorescence channels both showed that there were more Dox and TCPP were accumulating in Hela cells treated by DPN than that of DP treated cells. Based on the analysis of the previous experimental results, the ability of A549 and Hela cells to control the release of drug from PCN-224 MOF nanoparticles was basically the same, and the NPKMTX peptide modification would not affect the total release amount of Dox. Therefore, it can be concluded that the results of DPN treated Hela cell samples showed stronger fluorescence was due to the more cellular uptake of DPN by Hela cells. The results of the FACS experiment matched the results of the previous cytotoxicity experiments, further proving that the difference in the lethality of DPN against the three types of cells is due to the difference in cellular uptake, thereby verifying the targeting function of NPKMTX peptide modification.

4.2.3 Confocal laser scanning microscope (CLSM)

Confocal laser microscopy was used to observe the distribution of PCN-224 MOF nanoparticles and drugs at the subcellular level. Hela and A549 cells were treated with DP and DPN respectively, and then observed using a confocal microscope after PFA fixing. In the CLSM figures, the green color was chosen to represent TCPP fluorescence, and the red color to represent doxorubicin fluorescence. As shown in the **Figure 19 (a)**, the green and red fluorescence in the Hela cell sample treated with DPN was significantly stronger than the Hela sample treated with DP. Because doxorubicin is a small molecule drug, it should be easier to accumulate in the nucleus than MOF. It is obvious that there was prominent red fluorescence at the cell nucleus in the merge diagram, which is also proved by the fluorescence intensity distribution data in the diagram (**Figure 19 (b)**, **(c)**). In the Hela samples treated by DP, because the cells did not take up enough nanoparticles, the accumulation of the released dox fluorescence signal in the nucleus was not prominent. The fluorescence intensity distribution diagram showed that the fluorescence intensity of doxorubicin and TCPP at cell nucleus regions are not different obviously.

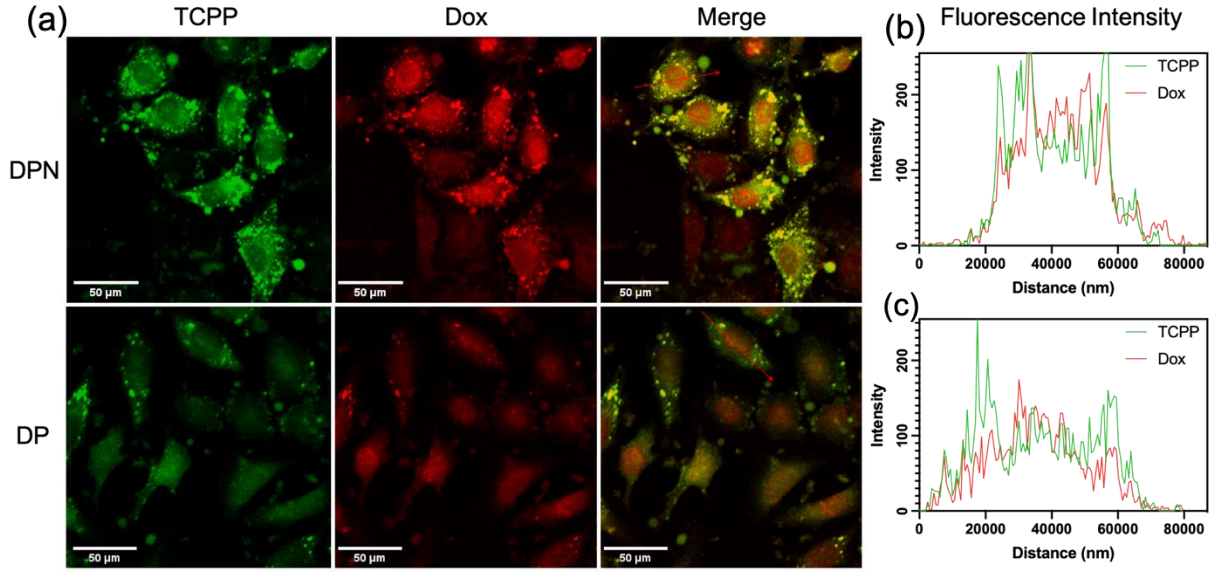

Figure 19 CLSM images and corresponding fluorescence histograms of cell uptake experiments on Hela cell line

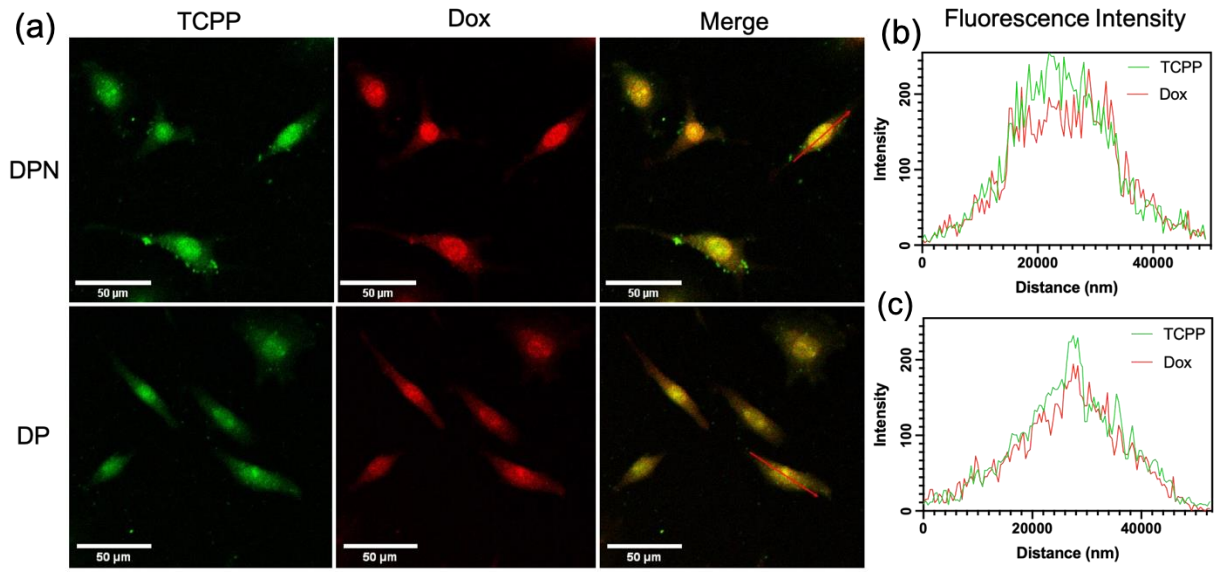

Figure 20 CLSM images and corresponding fluorescence histograms of cell uptake experiments on A549 cell line

In the CLSM pictures of A549 cells (**Figure 20 (a)**), we found that there is no significant difference in fluorescence intensity between DP and DPN-treated cell samples. The fluorescence signals in the DPN group are slightly stronger than that of the DP group, and some fluorescent bright spots can be observed outside the cell membrane. This may be because the NPKMTX polypeptide is positively charged and has some affinity with the negatively charged cell membrane. Similar to the DP-treated Hela cell sample, as shown in **Figure 20 (b)** and **(c)**, due to the limited number of nanoparticles taken up in the cell, the Dox fluorescence distribution in the nuclear area of A549 cells during the dosing time was not significantly different from that of TCPP.

In order to determine that more of the uptake of DPN by Hela cells is due to the active targeting effect of NPKMTX peptide on folate receptors, we conducted a competition experiment. The design idea of this experiment is to use FA to compete with MTX for FRs on the surface of Hela cells and to observe the amount of drug uptake by the cells to analyze whether NPKMTX peptide has a targeting effect on folate receptors. Two types of cells, A549 and Hela, were used as models. In addition to DP and DPN groups, DPN+FA and DP+FA groups were also added for comparison. As can be seen in **Figure 21**, the fluorescence intensity of Dox in the Hela cell sample treated with FA+DPN is significantly

lower than that of the DPN group, which is nearly 70%. The fluorescence intensity of dox in the cells in the other control groups remained basically unchanged. In **Figure 22**, the fluorescence intensity profiles of the four control groups of A549 cells are consistent. These results indicated NPKMTX peptide and FA competed for the FRs overexpressed in Hela cells, which further proves that the DPN drug delivery system can enter cancer cells through the active targeting effect of specifically recognizing folate receptors.

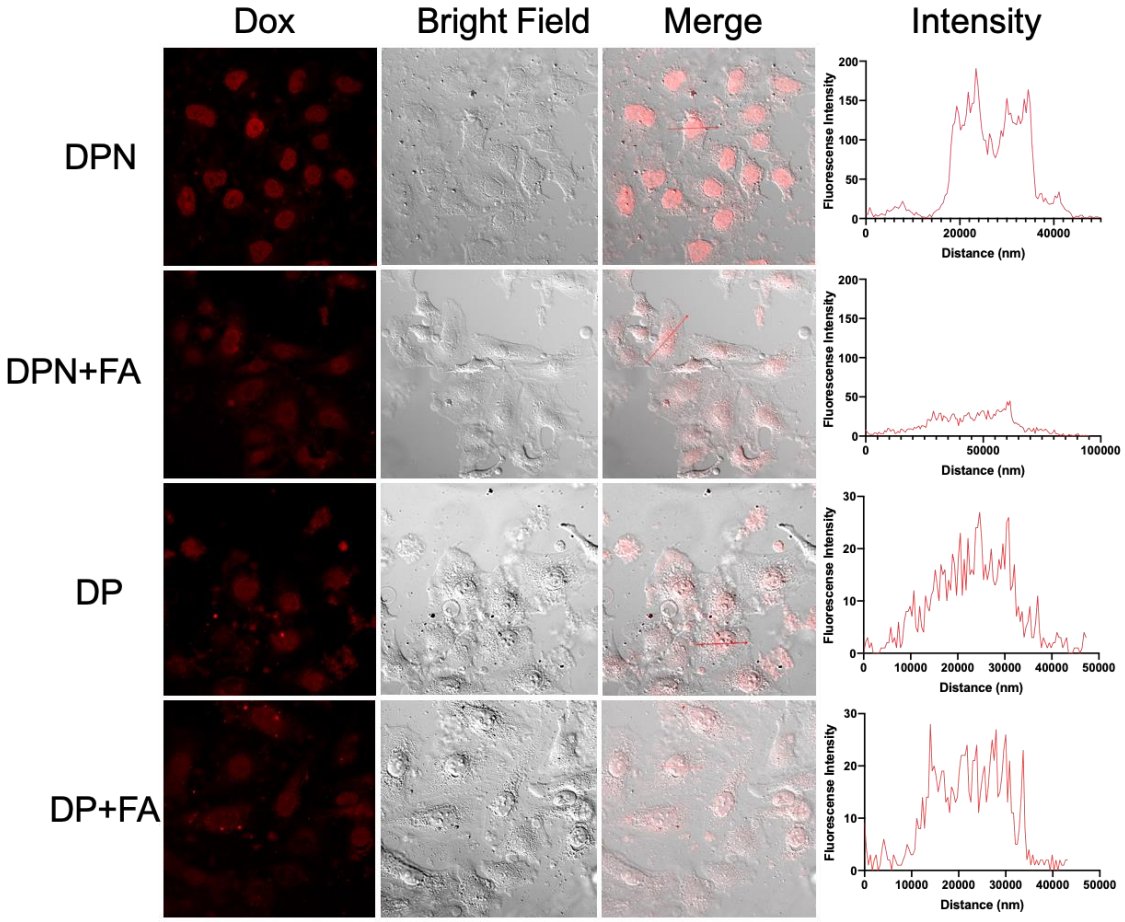

Figure 21 CLSM images and corresponding fluorescence histograms of competition experiment of DPN and FA on Hela cell line

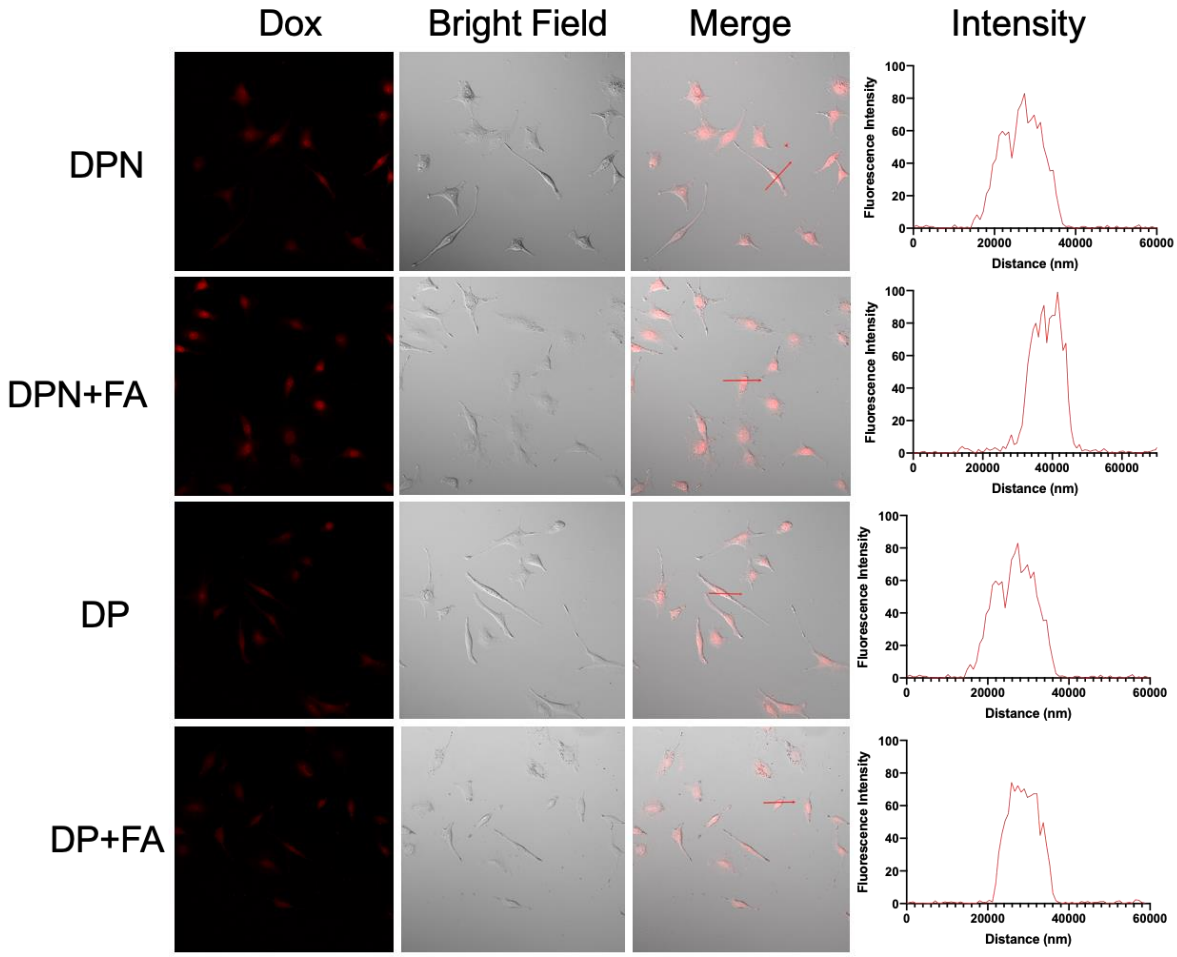

Figure 22 CLSM images and corresponding fluorescence histograms of competition experiment of DPN and FA on A549 cell line

4.3 Conclusions

Corresponding to the physical and chemical properties of the DPN drug delivery system, the cytotoxicity and cellular uptake properties of the system have been specially investigated. By introducing MTX molecules that can target folate receptors, NPKMTX peptide could be specifically recognized by folate receptors over-expressed on the surface of cancer cells. After the DPN complex was endocytosed by cancer cells, the histidine fragments induced the proton sponge effect and then were protonated. This led to the disassembly of the NPKMTX peptide and the release of the Dox encapsulated in PCN-224 MOF nanoparticles. The NPKMTX peptide that escaped from the endosome acted as a prodrug to release the MTX molecule during the degradation process in the lysosome. At the same time, cancer cells were irradiated by laser of a specific wavelength, TCPP in PCN-224 generated ROS to further kill cancer cells through photodynamic effect. The results of a series of cytotoxicity tests showed that the DPN drug delivery system showed great lethality against folate receptor positive cancer cells, while the damage to normal cells was controlled at a relatively low level. Both FACS and CLSM results showed that Dox and TCPP were more distributed in cancer cells with high folate receptor expression. Combined with the analysis of the cytotoxicity experiment results, it can be proved that the difference in the

toxicity of the DPN drug delivery system to different cells is due to the difference in cellular uptake. Competitive experiments further confirmed that the high uptake of DPN by Hela cells was due to the specific recognition of NPKMTX by FRs, thus proving the targeting function of the DPN system.

Chapter 5 Summary of Thesis and Recommendation for Future Work

In this thesis, we modified the NP1 peptide designed by our previous team members to make a new peptide named NPKMTX based on the shortcomings of the current anti-cancer drug delivery system. PCN-224 nano MOF particles and NPKMTX peptide were used to build the Dox@PCN-NPKMTX multifunctional anticancer drug delivery system for the targeted killing of cancer cells over-expressing folate receptors. PCN-224 nano MOF particles are biodegradable and adjustable in shape and size and exhibit high drug loading efficiency due to the porous structure. They can deliver anticancer drugs like Dox and the photosensitizer TCPP simultaneously. Therefore, PCN-224 nano MOF could be used as a potential drug delivery platform for chemotherapy and photodynamic therapy. However, the drug loaded inside would inevitably escape randomly during the delivery process in body fluids, which reduces the efficiency of drug delivery. On the other hand, nanoparticles can only passively target and accumulate in cancer cells through the EPR effect, which lacks the ability to actively target. NP1 peptide has been demonstrated its ability to self-assemble and encapsulate drugs; good cell membrane affinity and easy to complex internalization, but NP1 has no active targeting ability either. In order to enhance the specific lethality against tumor

cells while reducing side effects, MTX molecules were introduced into the NP1 sequence to achieve the function of targeting folate receptors. After escaping from the endosome, the NPKMTX peptide will be degraded in the lysosome as a prodrug to release the MTX molecule and achieve a dual-drug chemotherapy effect with Dox to reduce drug resistance. The test results showed that similar to the NP1 peptide, the NPKMTX peptide also has the ability of pH-regulated self-assembly (dis-assembly). The NPKMTX peptide coating layer modified on the surface of PCN-224 MOF nanoparticles can effectively prevent the random escape of Dox, and simultaneously help to achieve sustained drug release in a low pH environment. The cytotoxicity results showed that Dox@PCN-NPKMTX has a specific and great lethality against Hela cells with high folate receptor expression. The results of FACS and CLSM were also consistent with the cytotoxicity results, proving the active targeting function of the DPN system.

Since PCN-224 is a relatively classic MOF structure, other researchers have done PCN MOF-based drug delivery studies in their early research. For example, Kibeom with his colleagues modified PCN-224 MOF using hyaluronic acid to encapsulate dox [158]; Jihye's team synthesized PCN-224 nano particles with FA modification for targeting to Hela cells [116]; and DNA aptamer was also used to functionalize PCN MOF for targeting function by

Yuanchao [109] etc. Comparing with the work of other researchers, the DPN drug delivery system developed in this thesis has a series of advantages. In Jihye's project, folic acid which was used for targeting delivery of photosensitizer is also one of the important nutrients in the process of cancer cell proliferation. Folic acid molecules that enter cancer cells may help cancer cells grow, thereby reducing the effectiveness of photodynamic therapy. In our work, the use of the folic acid structural analogue MTX in the DPN drug delivery system not only can target the folate receptor, but also can be used as an anti-cancer drug to play the role of dual-drug chemotherapy together with dox while reducing tumor resistance. The dox release profile of HA-PCN system showed that the release amount of dox has reached the maximum value in 15 hours in acidic environment. This may trigger a cytokine storm and adversely affect the body. In DPN drug delivery system, NPKMTX peptide on MOF nano particle surface can slowly disassemble, thereby helping the drug to be released slowly within 72 hours, maintaining an effective drug concentration for a long time, and reducing drug concentration fluctuations and adverse reactions to the body. Yuanchao used DNA aptamer to functionalize PCN-224 MOF aiming to target to and selectively kill A549 cells. However, there was not a large difference between the cytotoxicity of their DNA-MOF complex to A549 cells and MCF7 cells. When the viability of A549 cells was 30%, the survival rate of

MCF7 was only 45%. In this thesis, DPN showed extremely strong selective killing ability to Hela cells. The results of the cytotoxicity experiment showed that when the viability Hela cells dropped to 30%, that of HEK293 cells compared with it could reach 80%. It indicates that the DPN drug delivery system may have a better targeting ability to accurately kill specific types of cancer cells.

There is still a lot of work that could be done to consummate this research. First of all, the mechanism of covalent bonding between NPKMTX peptide and PCN-224 MOF nanoparticles needs to be further researched. For example, X-ray photoelectron spectroscopy (XPS) can be used to measure the energy change of electrons on a specific orbital of Zr to indicate the formation of covalent bonds, isothermal titration calorimetry (ITC) can be used to measure the heat of reaction when covalent bonds are formed, and density functional theory (DFT) can be used for intermolecular interactions simulation, etc. These additional technical methods can help meticulous research and analysis of the mechanism of peptide modification of MOF. Since the DPN multifunctional drug delivery system has achieved good experimental results at the cellular level, the next stage of in vivo experiments can be designed to carry out research closer to practical applications.

References

[1]. Van Vleet, Weng, T., Li, X., & Schmidt, J. (2018). In Situ, Time-Resolved, and Mechanistic Studies of Metal–Organic Framework Nucleation and Growth. Chemical Reviews, 118(7), 3681–3721.

[2]. Sumida, Rogow, D. L., Mason, J. A., McDonald, T. M., Bloch, E. D., Herm, Z. R., Bae, T.-H., & Long, J. R. (2012). Carbon Dioxide Capture in Metal–Organic Frameworks. Chemical Reviews, 112(2), 724–781.

[3]. Taylor-Pashow, Rocca, J. D., Xie, Z., Tran, S., & Lin, W. (2009). Postsynthetic Modifications of Iron-Carboxylate Nanoscale Metal−Organic Frameworks for Imaging and Drug Delivery. Journal of the American Chemical Society, 131(40), 14261–14263.

[4]. Sun, Qin, C., Wang, C.-G., Su, Z.-M., Wang, S., Wang, X.-L., Yang, G.-S., Shao, K.-Z., Lan, Y.-Q., & Wang, E.-B. (2011). Chiral Nanoporous Metal-Organic Frameworks with High Porosity as Materials for Drug Delivery. Advanced Materials (Weinheim), 23(47), 5629–5632.

[5]. Meng, Gui, B., Yuan, D., Zeller, M., & Wang, C. (2016). Mechanized azobenzene-functionalized zirconium metal-organic framework for on-command cargo release. Science Advances, 2(8), e1600480–e1600480.

[6]. Bian, Wang, T., Zhang, L., Li, L., & Wang, C. (2015). A combination of tri-modal cancer imaging and in vivo drug delivery by metal-organic framework based composite nanoparticles. Biomaterials Science, 3(9), 127–1278.

[7]. AbouAitah, K., Swiderska-Sroda, A., Farghali, A. A., Wojnarowicz, J., Stefanek, A., Gierlotka, S., ... & Lojkowski, W. (2018). Folic acid–conjugated mesoporous silica particles as nanocarriers of natural prodrugs for cancer targeting and antioxidant action. Oncotarget, 9(41), 26466.

[8]. Sanna, Pala, N., & Sechi, M. (2014). Targeted therapy using nanotechnology: Focus on cancer. International Journal of Nanomedicine, 9(1), 467–483.

[9]. Tang, & Cheng, J. (2013). Nonporous silica nanoparticles for nanomedicine application. Nano Today, 8(3), 290–312.

[10]. Adair. (2018). Characterization of Calcium Phosphosilicate (Hydrate) Nanoparticles: Novel Organic-Inorganic Composite Nanomaterial for Drug and Diagnostic Delivery. Microscopy and Microanalysis, 24(S1), 1252–1253.

[11]. Debele, T. A., Peng, S., & Tsai, H. C. (2015). Drug carrier for photodynamic cancer therapy. International journal of molecular sciences, 16(9), 22094-22136.

[12]. Van Vleet, Weng, T., Li, X., & Schmidt, J. (2018). In Situ, Time-Resolved, and Mechanistic Studies of Metal–Organic Framework Nucleation and Growth. Chemical Reviews, 118(7), 3681–3721.

[13]. Kundu, Mitra, S., Patra, P., Goswami, A., Díaz Díaz, D., & Banerjee, R. (2014). Mechanical Downsizing of a Gadolinium (III)-based Metal-Organic Framework for Anticancer Drug Delivery. Chemistry: a European Journal, 20(33), 10514–10518.

[14]. Bloch, E. D., Queen, W. L., Krishna, R., Zadrozny, J. M., Brown, C. M., & Long, J. R. (2012). Hydrocarbon separations in a metal-organic framework with open iron (II) coordination sites. Science (New York, N.Y.), 335(6076), 1606–1610.

[15]. Moghimi, S. M., Hunter, A. C., & Murray, J. C. (2001). Long-circulating and target-specific nanoparticles: theory to practice. Pharmacological reviews, 53(2), 283-318.

[16]. Kalyane, D., Raval, N., Maheshwari, R., Tambe, V., Kalia, K., & Tekade, R. K. (2019). Employment of enhanced permeability and retention effect (EPR): Nanoparticle-based precision tools for targeting of therapeutic and diagnostic agent in cancer. Materials Science and Engineering: C, 98, 1252-1276.

[17]. Nakamura, Y., Mochida, A., Choyke, P. L., & Kobayashi, H. (2016). Nanodrug Delivery: Is the Enhanced Permeability and Retention Effect Sufficient for Curing Cancer?. Bioconjugate chemistry, 27(10), 2225–2238.

[18]. Shi, Y., van der Meel, R., Chen, X., & Lammers, T. (2020). The EPR effect and beyond: Strategies to improve tumor targeting and cancer nanomedicine treatment efficacy. Theranostics, 10(17), 7921–7924.

[19]. Silva, P., Vilela, S. M., Tomé, J. P., & Almeida Paz, F. A. (2015). Multifunctional metal-organic frameworks: from academia to industrial applications. Chemical Society reviews, 44(19), 6774–6803.

[20]. Ma, S., Zhou, J., Wali, A. R., He, Y., Xu, X., Tang, J. Z., & Gu, Z. (2015). Self-assembly of pH-sensitive fluorinated peptide dendron functionalized dextran nanoparticles for on-demand intracellular drug delivery. Journal of materials science. Materials in medicine, 26(8), 219.

[21]. Molina, M., Asadian-Birjand, M., Balach, J., Bergueiro, J., Miceli, E., & Calderón, M. (2015). Stimuli-responsive nanogel composites and their application in nanomedicine. Chemical Society reviews, 44(17), 6161–6186.

[22]. Huang, C., Li, A., Chen, X., & Wang, T. (2020). Understanding the Role of Metal–Organic Frameworks in Surface-Enhanced Raman Scattering Application. Small, 16(43), 2004802.

[23]. Jiang, K., Zhang, L., Hu, Q., Zhao, D., Xia, T., Lin, W., ... & Qian, G. (2016). Pressure controlled drug release in a Zr-cluster-based MOF. Journal of Materials Chemistry B, 4(39), 6398-6401.

[24]. An, J., Geib, S. J., & Rosi, N. L. (2009). Cation-triggered drug release from a porous zinc− adeninate metal− organic framework. *Journal of the American Chemical Society*, *131*(24), 8376-8377.

[25]. Wu, M. X., Gao, J., Wang, F., Yang, J., Song, N., Jin, X., ... & Yang, Y. W. (2018). Multistimuli responsive core–shell nanoplatform constructed from Fe3O4@ MOF equipped with pillar [6] arene nanovalves. Small, 14(17), 1704440.

[26]. He, L., Liu, Y., Lau, J., Fan, W., Li, Q., Zhang, C., ... & Chen, X. (2019). Recent progress in nanoscale metal-organic frameworks for drug release and cancer therapy. *Nanomedicine*, *14*(10), 1343-1365.

[27]. Wang, Y., Yan, J., Wen, N., Xiong, H., Cai, S., He, Q., ... & Liu, Y. (2020). Metal-organic frameworks for stimuli-responsive drug delivery. Biomaterials, 230, 119619.

[28]. Taylor-Pashow, K. M., Della Rocca, J., Xie, Z., Tran, S., & Lin, W. (2009). Postsynthetic modifications of iron-carboxylate nanoscale metal-organic frameworks for imaging and drug delivery. Journal of the American Chemical Society, 131(40), 14261–14263.

[29]. Agostinis, P., Berg, K., Cengel, K. A., Foster, T. H., Girotti, A. W., Gollnick, S. O., ... & Golab, J. (2011). Photodynamic therapy of cancer: an update. CA: a cancer journal for clinicians, 61(4), 250-281.

[30]. Dolmans, D. E., Fukumura, D., & Jain, R. K. (2003). Photodynamic therapy for cancer. Nature reviews. Cancer, 3(5), 380–387.

[31]. Ethirajan, M., Chen, Y., Joshi, P., & Pandey, R. K. (2011). The role of porphyrin chemistry in tumor imaging and photodynamic therapy. Chemical Society reviews, 40(1), 340–362.

[32]. Lovell, J. F., Liu, T. W., Chen, J., & Zheng, G. (2010). Activatable photosensitizers for imaging and therapy. Chemical reviews, 110(5), 2839–2857.

[33]. Agostinis, P., Berg, K., Cengel, K. A., Foster, T. H., Girotti, A. W., Gollnick, S. O., ... & Golab, J. (2011). Photodynamic therapy of cancer: an update. CA: a cancer journal for clinicians, 61(4), 250-281.

[34]. Yang, H., Lou, C., Xu, M., Wu, C., Miyoshi, H., & Liu, Y. (2011). Investigation of folate-conjugated fluorescent silica nanoparticles for targeting delivery to folate receptor-positive tumors and their internalization mechanism. International journal of nanomedicine, 6, 2023–2032.

[35]. Weinstein, S. J., Hartman, T. J., Stolzenberg-Solomon, R., Pietinen, P., Barrett, M. J., Taylor, P. R., Virtamo, J., & Albanes, D. (2003). Null association between prostate cancer and serum folate, vitamin B (6), vitamin B (12), and homocysteine. Cancer epidemiology, biomarkers & prevention: a publication of the American Association for Cancer Research, cosponsored by the American Society of Preventive Oncology, 12(11 Pt 1), 1271–1272.

[36]. Lu, Y., & Low, P. S. (2002). Folate-mediated delivery of macromolecular anticancer therapeutic agents. Advanced drug delivery reviews, 54(5), 675–693.

[37]. Miller, J. W., Borowsky, A. D., Marple, T. C., McGoldrick, E. T., Dillard-Telm, L., Young, L. J., & Green, R. (2008). Folate, DNA methylation, and mouse models of breast tumorigenesis. Nutrition reviews, 66 Suppl 1(0 1), S59–S64.

[38]. Koźmiński, P., Halik, P. K., Chesori, R., & Gniazdowska, E. (2020). Overview of Dual-Acting Drug Methotrexate in Different Neurological Diseases, Autoimmune Pathologies and Cancers. International journal of molecular sciences, 21(10), 3483.

[39]. Inoue, K., & Yuasa, H. (2014). Molecular basis for pharmacokinetics and pharmacodynamics of methotrexate in rheumatoid arthritis therapy. Drug metabolism and pharmacokinetics, 29(1), 12–19.

[40]. Wong, P. T., & Choi, S. K. (2015). Mechanisms and implications of dual-acting methotrexate in folate-targeted nanotherapeutic delivery. International journal of molecular sciences, 16(1), 1772–1790.

[41]. Theti, D. S., & Jackman, A. L. (2004). The role of alpha-folate receptor-mediated transport in the antitumor activity of antifolate drugs. Clinical cancer research : an official journal of the American Association for Cancer Research, 10(3), 1080–1089.

[42]. Wang, J., Liu, K., Xing, R., & Yan, X. (2016). Peptide self-assembly: thermodynamics and kinetics. Chemical Society Reviews, 45(20), 5589-5604.

[43]. Liang W, Lam JKW (2012) Endosomal escape pathways for non-viral nucleic acid delivery systems. In: Ceresa B (ed) Molecular regulation of endocytosis.

[44]. Deshayes, S., Konate, K., Rydström, A., Crombez, L., Godefroy, C., Milhiet, P. E., ... & Divita, G. (2012). Self‐Assembling Peptide‐Based Nanoparticles for siRNA Delivery in Primary Cell Lines. Small, 8(14), 2184-2188.

[45]. Maeda, H., Nakamura, H., & Fang, J. (2013). The EPR effect for macromolecular drug delivery to solid tumors: Improvement of tumor uptake, lowering of systemic toxicity, and distinct tumor imaging in vivo. Advanced drug delivery reviews, 65(1), 71–79.

[46]. Boisguérin, P., Deshayes, S., Gait, M. J., O'Donovan, L., Godfrey, C., Betts, C. A., Wood, M. J., & Lebleu, B. (2015). Delivery of therapeutic oligonucleotides with cell penetrating peptides. Advanced drug delivery reviews, 87, 52–67.

[47]. Komin, A., Russell, L. M., Hristova, K. A., & Searson, P. C. (2017). Peptide-based strategies for enhanced cell uptake, transcellular transport, and circulation: Mechanisms and challenges. Advanced drug delivery reviews, 110-111, 52–64.

[48]. Ma, D. (2014). Enhancing endosomal escape for nanoparticle mediated siRNA delivery. Nanoscale, 6(12), 6415-6425.

[49]. Pärnaste, Ly, Arukuusk, Piret, Langel, Kent, Tenson, Tanel, & Langel, Ülo. (2017). The Formation of Nanoparticles between Small Interfering RNA and Amphipathic Cell-Penetrating Peptides. Molecular Therapy - Nucleic Acids, 7(C), 1-10.

[50]. M. Aliabadi, Landry, Sun, Tang, & Uludağ. (2011). Supramolecular assemblies in functional siRNA delivery: Where do we stand? Biomaterials, 33(8), 2546-2569.

[51]. Ruoslahti E. (2017). Tumor penetrating peptides for improved drug delivery. Advanced drug delivery reviews, 110-111, 3–12.

[52]. Wang, F., Wang, Y., Zhang, X., Zhang, W., Guo, S., & Jin, F. (2014). Recent progress of cell-penetrating peptides as new carriers for intracellular cargo delivery. Journal of controlled release: official journal of the Controlled Release Society, 174, 126 - 136.

[53]. Chu, D., Xu, W., Pan, R., Ding, Y., Sui, W., & Chen, P. (2015). Rational modification of oligoarginine for highly efficient siRNA delivery: structure-activity relationship and mechanism of intracellular trafficking of siRNA. Nanomedicine: nanotechnology, biology, and medicine, 11(2), 435–446.

[54]. Chu, Xu, W., Pan, R., & Chen, P. (2015). Co-delivery of drug nanoparticles and siRNA mediated by a modified cell penetrating peptide for inhibiting cancer cell proliferation. RSC Advances, 5(26), 20554–20556.

[55]. Deshayes, S., Konate, K., Rydström, A., Crombez, L., Godefroy, C., Milhiet, P. E., ... & Divita, G. (2012). Self - Assembling Peptide - Based Nanoparticles for siRNA Delivery in Primary Cell Lines. Small, 8(14), 2184-2188.

[56]. Herce, H., Garcia, A., & Cardoso, M. (2014). Fundamental molecular mechanism for the cellular uptake of guanidinium-rich molecules. 136(50), 17459-17467.

[57]. Rothbard, J., Jessop, T., Lewis, R., Murray, B., & Wender, P. (2004). Role of Membrane Potential and Hydrogen Bonding in the Mechanism of Translocation of Guanidinium-Rich Peptides into Cells. Journal of the American Chemical Society, 126(31), 9506-9507.

[58]. Borrelli, A., Tornesello, A. L., Tornesello, M. L., & Buonaguro, F. M. (2018). Cell penetrating peptides as molecular carriers for anti-cancer agents. Molecules, 23(2), 295.

[59]. Lo, & Wang, S. (2012). Evaluation of the use of amphipathic peptide-based protein carrier for in vitro cancer research. Biochemical and Biophysical Research Communications, 419(2), 170–174.

[60]. Oggianu, Monni, N., Mameli, V., Cannas, C., Sahadevan, S. A., & Mercuri, M. L. (2020). Designing magnetic nanomofs for biomedicine: Current trends and applications. Magnetochemistry, 6(3), 1–14.

[61]. Sun, J., Wang, J., & Yang, Z. (2015). Supramolecular Assembly Models of siRNA Delivery Systems. Chinese Journal of Chemistry, 33(1), 79-89.

[62]. Liang W, Lam JKW (2012) Endosomal escape pathways for non-viral nucleic acid delivery systems. In: Ceresa B (ed) Molecular regulation of endocytosis.

[63]. Tan, Jia, X., Jiang, X., Zhang, Y., Tang, H., Yao, S., & Xie, Q. (2009). In vitro study on the individual and synergistic cytotoxicity of adriamycin and selenium nanoparticles against Bel7402 cells with a quartz crystal microbalance. Biosensors & Bioelectronics, 24(7), 2268–2272.

[64]. Wang, C., Cheng, L., & Liu, Z. (2011). Drug delivery with upconversion nanoparticles for multi-functional targeted cancer cell imaging and therapy. Biomaterials, 32(4), 1110-1120.

[65]. Kayal, S., & Ramanujan, R. V. (2010). Doxorubicin loaded PVA coated iron oxide nanoparticles for targeted drug delivery. Materials Science and Engineering: C, 30(3), 484-490.

[66]. Yang, X., Hong, H., Grailer, J. J., Rowland, I. J., Javadi, A., Hurley, S. A., ... & Gong, S. (2011). cRGD-functionalized, DOX-conjugated, and 64Cu-labeled superparamagnetic iron oxide nanoparticles for targeted anticancer drug delivery and PET/MR imaging. Biomaterials, 32(17), 4151-4160.

[67]. Zheng, C., Wang, Y., Phua, S. Z. F., Lim, W. Q., & Zhao, Y. (2017). ZnO–DOX@ ZIF-8 core–shell nanoparticles for pH-responsive drug delivery. ACS Biomaterials Science & Engineering, 3(10), 2223-2229.

[68]. Liu, Yang, Y., Zhu, W., Yi, X., Dong, Z., Xu, X., Chen, M., Yang, K., Lu, G., Jiang, L., & Liu, Z. (2016). Nanoscale metal−organic frameworks for combined photodynamic & radiation therapy in cancer treatment. Biomaterials, 97, 1–9.

[69]. Bukhtoyarov, O. V., & Samarin, D. M. (2015). Pathogenesis of cancer: Cancer reparative trap. Journal of Cancer Therapy, 6(05), 399.

[70]. Solomon, Kim, J.-S., & Waldman, T. (2014). Cohesin gene mutations in tumorigenesis: From discovery to clinical significance. BMB Reports, 47(6), 299–310.

[71]. Yang, & Bialkowska, A. B. (2015). Intestinal Tumorigenesis Mechanisms of Development & Progression (1st ed. 2015.). Springer International Publishing.

[72]. Whiteside, T. L. (2008). The tumor microenvironment and its role in promoting tumor growth. Oncogene, 27(45), 5904-5912.

[73]. Dasari, & Bernard Tchounwou, P. (2014). Cisplatin in cancer therapy: Molecular mechanisms of action. European Journal of Pharmacology, 740, 364–378.

[74]. Janssen, & Medema, R. (2011). Mitosis as an anti-cancer target. Oncogene, 30(25), 2799–2809.

[75]. Wu, X. Z. (2006). A new classification system of anticancer drugs–based on cell biological mechanisms. Medical Hypotheses, 66(5), 883-887.

[76]. Gibbs, J. B. (2000). Mechanism-based target identification and drug discovery in cancer research. Science, 287(5460), 1969-1973.

[77]. Wang, Y., & Chen, Z. (2020). Mutation detection and molecular targeted tumor therapies. STEMedicine, 1(1), e11-e11.

[78]. Wen, D. O. N. G., Yan, Z. H. O. U., & Jin-an, M. A. (2013). The Molecular Typing and Targeted Therapy of Lung Adenocarcinoma with Genetic Variations. Medical Recapitulate, 09.

[79]. Hayes, D. F., Bast, R. C., Desch, C. E., Fritsche Jr, H., Kemeny, N. E., Jessup, J. M., ... & Winn, R. J. (1996). Tumor marker utility grading system: a framework to evaluate clinical utility of tumor markers. JNCI: Journal of the National Cancer Institute, 88(20), 1456-1466.

[80]. Sharma, S. (2009). Tumor markers in clinical practice: General principles and guidelines. Indian journal of medical and paediatric oncology: official journal of Indian Society of Medical & Paediatric Oncology, 30(1), 1.

[81]. Wang, Liu, H., Pei, L., Wang, K., Song, C., Wang, P., Ye, H., Zhang, J., Ji, Z., Ouyang, S., & Dai, L. (2020). Screening of tumor-associated antigens based on Oncomine database and evaluation of diagnostic value of autoantibodies in lung cancer. Clinical Immunology (Orlando, Fla.), 210, 108262–108262.

[82]. Sarandakou, A., Protonotariou, E., & Rizos, D. (2007). Tumor markers in biological fluids associated with pregnancy. Critical reviews in clinical laboratory sciences, 44(2), 151-178.

[83]. Ding, Zhang, W., Wang, W., Chen, Y., & Li, X. (2015). Amplification strategies using electrochemiluminescence biosensors for the detection of DNA, bioactive molecules and cancer biomarkers. TrAC, Trends in Analytical Chemistry (Regular Ed.), 65, 137–150.

[84]. Tacar, Sriamornsak, P., & Dass, C. R. (2013). Doxorubicin: an update on anticancer molecular action, toxicity and novel drug delivery systems. Journal of Pharmacy and Pharmacology, 65(2), 157–170.

[85]. Pegoraro, Cecchin, D., Gracia, L. S., Warren, N., Madsen, J., Armes, S. P., Lewis, A., MacNeil, S., & Battaglia, G. (2013). Enhanced drug delivery to melanoma cells using PMPC-PDPA polymersomes. Cancer Letters, 334(2), 328–337.

[86]. Fu, Pan, H., Tang, Y., Rong, J., & Zheng, Z. (2021). MiR-200a-3p Aggravates DOX-Induced Cardiotoxicity by Targeting PEG3 Through SIRT1/NF-κB Signal Pathway. Cardiovascular Toxicology, 21(4), 302–313.

[87]. Ledzewicz, U., & Schättler, H. (2006). Drug resistance in cancer chemotherapy as an optimal control problem. Discrete & Continuous Dynamical Systems-B, 6(1), 129.

[88]. Yao, Y., Zhou, Y., Liu, L., Xu, Y., Chen, Q., Wang, Y., ... & Shao, A. (2020). Nanoparticle-based drug delivery in cancer therapy and its role in overcoming drug resistance. Frontiers in Molecular Biosciences, 7.

[89]. Shi, Ho, K., Keating, A., & Shoichet, M. S. (2009). Anticancer Drug Delivery: Doxorubicin-Conjugated Immuno-Nanoparticles for Intracellular Anticancer Drug Delivery (Adv. Funct. Mater. 11/2009). Advanced Functional Materials, 19(11).

[90]. Huang, Z. (2005). A review of progress in clinical photodynamic therapy. Technology in cancer research & treatment, 4(3), 283-293.

[91]. Zhu, T. C., & Finlay, J. C. (2008). The role of photodynamic therapy (PDT) physics. Medical physics, 35(7Part1), 3127-3136.

[92]. Allison, R., Moghissi, K., Downie, G., & Dixon, K. (2011). Photodynamic therapy (PDT) for lung cancer. Photodiagnosis and photodynamic therapy, 8(3), 231-239.

[93]. Sun, Z., Zhang, L. P., Wu, F., & Zhao, Y. (2017). Photosensitizers for two-photon excited photodynamic therapy. Advanced Functional Materials, 27(48), 1704079.

[94]. Bretin, L., Pinon, A., Bouramtane, S., Ouk, C., Richard, L., Perrin, M. L., ... & Liagre, B. (2019). Photodynamic therapy activity of new porphyrin-xylan-coated silica nanoparticles in human colorectal cancer. Cancers, 11(10), 1474.

[95]. Dougherty, Gomer, C. J., Jori, G., Kessel, D., Korbelik, M., Moan, J., & Peng, Q. (1998). Photodynamic Therapy. JNCI: Journal of the National Cancer Institute, 90(12), 889–905.

[96]. Li, X., Vinothini, K., Ramesh, T., Rajan, M., & Ramu, A. (2020). Combined photodynamic-chemotherapy investigation of cancer cells using carbon quantum dot-based drug carrier system. Drug delivery, 27(1), 791-804.

[97]. M. Aliabadi, Landry, Sun, Tang, & Uludağ. (2011). Supramolecular assemblies in functional siRNA delivery: Where do we stand? Biomaterials, 33(8), 2546-2569.

[98]. Oggianu, M., Monni, N., Mameli, V., Cannas, C., Ashoka Sahadevan, S., & Mercuri, M. L. (2020). Designing Magnetic NanoMOFs for Biomedicine: Current Trends and Applications. Magnetochemistry, 6(3), 39.

[99]. Sun, J., Wang, J., & Yang, Z. (2015). Supramolecular Assembly Models of siRNA Delivery Systems. Chinese Journal of Chemistry, 33(1), 79-89.

[100]. Ding, Zhang, W., Wang, W., Chen, Y., & Li, X. (2015). Amplification strategies using electrochemiluminescence biosensors for the detection of DNA, bioactive molecules and cancer biomarkers. TrAC, Trends in Analytical Chemistry (Regular Ed.), 65, 137–150.

[101]. Liu, Yang, Y., Zhu, W., Yi, X., Dong, Z., Xu, X., Chen, M., Yang, K., Lu, G., Jiang, L., & Liu, Z. (2016). Nanoscale metal−organic frameworks for combined photodynamic & radiation therapy in cancer treatment. Biomaterials, 97, 1–9.

[102]. Janssen, & Medema, R. (2011). Mitosis as an anti-cancer target. Oncogene, 30(25), 2799–2809.

[103]. Bukhtoyarov, O. V., & Samarin, D. M. (2015). Pathogenesis of cancer: Cancer reparative trap. Journal of Cancer Therapy, 6(05), 399.

[104]. Solomon, Kim, J.-S., & Waldman, T. (2014). Cohesin gene mutations in tumorigenesis: From discovery to clinical significance. BMB Reports, 47(6), 299–310.

[105]. Yang, & Bialkowska, A. B. (2015). Intestinal Tumorigenesis Mechanisms of Development & Progression (1st ed. 2015.). Springer International Publishing.

[106]. Thomas-Tikhonenko. (2009). Cancer Genome and Tumor Microenvironment. Springer New York.

[107]. Li, G., Pei, M., & Liu, P. (2020). DOX-conjugated CQD-based nanosponges for tumor intracellular pH-triggered DOX release and imaging. Colloids and Surfaces A: Physicochemical and Engineering Aspects, 603, 125258.

[108]. Wu, X. Z. (2006). A new classification system of anticancer drugs–based on cell biological mechanisms. Medical Hypotheses, 66(5), 883-887.

[109]. Zhang, Y., Wang, Q., Chen, G., & Shi, P. (2019). DNA-functionalized metal–organic framework: cell imaging, targeting drug delivery and photodynamic therapy. Inorganic chemistry, 58(10), 6593-6596.

[110]. Wang, Y., & Chen, Z. (2020). Mutation detection and molecular targeted tumor therapies. STEMedicine, 1(1), e11-e11.

[111]. Sarandakou, A., Protonotariou, E., & Rizos, D. (2007). Tumor markers in biological fluids associated with pregnancy. Critical reviews in clinical laboratory sciences, 44(2), 151-178.

[112]. Tacar, Sriamornsak, P., & Dass, C. R. (2013). Doxorubicin: an update on anticancer molecular action, toxicity and novel drug delivery systems. Journal of Pharmacy and Pharmacology, 65(2), 157–170.

[113]. Fu, Q., Pan, H., Tang, Y., Rong, J., & Zheng, Z. (2021). MiR-200a-3p Aggravates DOX-Induced Cardiotoxicity by Targeting PEG3 Through SIRT1/NF-κB Signal Pathway. Cardiovascular toxicology, 21(4), 302–313.

[114]. Yao, Y., Zhou, Y., Liu, L., Xu, Y., Chen, Q., Wang, Y., ... & Shao, A. (2020). Nanoparticle-based drug delivery in cancer therapy and its role in overcoming drug resistance. Frontiers in Molecular Biosciences, 7.

[115]. Wang, Z., Sun, Q., Liu, B., Kuang, Y., Gulzar, A., He, F., ... & Lin, J. (2021). Recent advances in porphyrin-based MOFs for cancer therapy and diagnosis therapy. Coordination Chemistry Reviews, 439, 213945.

[116]. Park, J., Jiang, Q., Feng, D., Mao, L., & Zhou, H. C. (2016). Size-controlled synthesis of porphyrinic metal–organic framework and functionalization for targeted photodynamic therapy. Journal of the American Chemical Society, 138(10), 3518-3525.

[117]. Li, S. Y., Cheng, H., Qiu, W. X., Zhang, L., Wan, S. S., Zeng, J. Y., & Zhang, X. Z. (2017). Cancer cell membrane-coated biomimetic platform for tumor targeted photodynamic therapy and hypoxia-amplified bioreductive therapy. Biomaterials, 142, 149-161.

[118]. Huang, Z. (2005). A review of progress in clinical photodynamic therapy. Technology in cancer research & treatment, 4(3), 283-293.

[119]. Zhu, T. C., & Finlay, J. C. (2008). The role of photodynamic therapy (PDT) physics. Medical physics, 35(7Part1), 3127-3136.

[120]. Allison, R., Moghissi, K., Downie, G., & Dixon, K. (2011). Photodynamic therapy (PDT) for lung cancer. Photodiagnosis and photodynamic therapy, 8(3), 231-239.

[121]. Sun, Z., Zhang, L. P., Wu, F., & Zhao, Y. (2017). Photosensitizers for two-photon excited photodynamic therapy. Advanced Functional Materials, 27(48), 1704079.

[122]. Li, G., Pei, M., & Liu, P. (2020). DOX-conjugated CQD-based nanosponges for tumor intracellular pH-triggered DOX release and imaging. Colloids and Surfaces A: Physicochemical and Engineering Aspects, 603, 125258.

[123]. Yang, Hu, Y., & Wang, H. (2016). Targeting Antitumor Immune Response for Enhancing the Efficacy of Photodynamic Therapy of Cancer: Recent Advances and Future Perspectives. Oxidative Medicine and Cellular Longevity, 2016, 5274084–11.

[124]. Yang, J., An, H. W., & Wang, H. (2020). Self-Assembled Peptide Drug Delivery Systems. ACS Applied Biomaterials, 4(1), 24-46.

[125]. Chen, H., & Stoddart, J. F. (2021). From molecular to supramolecular electronics. Nature Reviews Materials, 1-25.

[126]. Chibh, S., Mishra, J., Kour, A., Chauhan, V. S., & Panda, J. J. (2020). Recent advances in the fabrication and bio-medical applications of self-assembled dipeptide nanostructures. Nanomedicine, 16(2), 139-163.

[127]. Wang, J., Liu, K., Xing, R., & Yan, X. (2016). Peptide self-assembly: thermodynamics and kinetics. Chemical Society Reviews, 45(20), 5589-5604.

[128]. Cui, H., Webber, M. J., & Stupp, S. I. (2010). Self-assembly of peptide amphiphiles: From molecules to nanostructures to biomaterials. Peptide Science: Original Research on Biomolecules, 94(1), 1-18.

[129]. Borrelli, A., Tornesello, A. L., Tornesello, M. L., & Buonaguro, F. M. (2018). Cell penetrating peptides as molecular carriers for anti-cancer agents. Molecules, 23(2), 295.

[130]. Chen, Braun, G. B., Luo, X., Sugahara, K. N., Teesalu, T., & Ruoslahti, E. (2013). Application of a proapoptotic peptide to intratumorally spreading cancer therapy. Cancer Research (Chicago, Ill.), 73(4), 1352–1361.

[131]. Deepak Raina, Surender Kharbanda, Donald Kufe, & Yasumitsu Uchida. (2013). Inhibition of the MUC1-C oncoprotein is synergistic with cytotoxic agents in the treatment of breast cancer cells. Cancer Biology & Therapy, 14(2), 0–1.

[132]. Davis, M. E., Hsieh, P. C., Takahashi, T., Song, Q., Zhang, S., Kamm, R. D., ... & Lee, R. T. (2006). Local myocardial insulin-like growth factor 1 (IGF-1) delivery with biotinylated peptide nanofibers improves cell therapy for myocardial infarction. Proceedings of the National Academy of Sciences, 103(21), 8155-8160.

[133]. Zhang, L., Xu, J., Wang, F., Ding, Y., Wang, T., Jin, G., ... & Chen, P. (2019). Histidine-rich cell-penetrating peptide for cancer drug delivery and its uptake mechanism. Langmuir, 35(9), 3513-3523.

[134]. Xu, W. (2014) Endosomolytic arginine-rich peptides for therapeutic siRNA delivery. Waterloo, Ontario, Canada: University of Waterloo.

[135]. Zhang, L. et al. (2019) Histidine-Rich Cell-Penetrating Peptide for Cancer Drug Delivery and Its Uptake Mechanism. Langmuir. [Online] 35 (9), 3513–3523.

[136]. Troiber, Kasper, J. C., Milani, S., Scheible, M., Martin, I., Schaubhut, F., Küchler, S., Rädler, J., Simmel, F. C., Friess, W., & Wagner, E. (2013). Comparison of four different particle sizing methods for siRNA polyplex characterization. European Journal of Pharmaceutics and Biopharmaceutics, 84(2), 255–264.

[137]. Hardy, Kamphuis, Japaridze, Wilschut, & Winterhalter. (2012). Nanoaggregates of micropurified lipopolysaccharide identified using dynamic light scattering, zeta potential measurement, and TLR4 signaling activity. Analytical Biochemistry, 430(2), 203-213.

[138]. Circular Dichroism. (2020, August 15). Retrieved July 20, 2021

[139]. Fluorescence and Phosphorescence. (2020, August 15). Retrieved July 20, 2021

[140]. Harris, D. C., & Bertolucci, M. D. (1989). Symmetry and spectroscopy: an introduction to vibrational and electronic spectroscopy. Courier Corporation.

[141]. Rajendran, M. (2016). Quinones as photosensitizer for photodynamic therapy: ROS generation, mechanism and detection methods. Photodiagnosis and photodynamic therapy, 13, 175-187.

[142]. Tang, X., Zhou, S., Tao, X., Wang, J., Wang, F., & Liang, Y. (2017). Targeted delivery of docetaxel via Pi Pi stacking stabilized dendritic polymeric micelles for enhanced therapy of liver cancer. Materials science and engineering: C, 75, 1042-1048.

[143]. Zeng, R., He, T., Lu, L., Li, K., Luo, Z., & Cai, K. (2021). Ultra-thin metal–organic framework nanosheets for chemo-photodynamic synergistic therapy. Journal of Materials Chemistry B, 9(20), 4143-4153.

[144]. Bagrov, D., Gazizova, Y., Podgorsky, V., Udovichenko, I., Danilkovich, A., Prusakov, K., & Klinov, D. (2016). Morphology and aggregation of RADA‐16‐I peptide Studied by AFM, NMR and molecular dynamics simulations. Peptide Science, 106(1), 72-81.

[145]. Norlin, Hellberg, M., Filippov, A., Sousa, A. A., Gröbner, G., Leapman, R. D., Almqvist, N., & Antzutkin, O. N. (2012). Aggregation and fibril morphology of the Arctic

mutation of Alzheimer's Aβ peptide by CD, TEM, STEM and in situ AFM. Journal of Structural Biology, 180(1), 174–189.

[146]. Volland. (2016). Scanning Electron Microscopy for the Life Sciences H. Schatten (ed.) New York: Cambridge University Press, 2013. 298pp. ISBN: 978‐0‐521‐19599‐7.

[147]. Stokes, Debbie J. (2008). Principles and Practice of Variable Pressure Environmental Scanning Electron Microscopy (VP-ESEM). Chichester: John Wiley & Sons. ISBN 978-0470758748.

[148]. Nishath, P. M., Sekar, K., Shameer, P. M., Usman, K. M., Shitu, A., Mary, J. S., & Dhinesh, B. (2020). Influence of pyrogallol (PY) antioxidant in the fuel stability of alexandrian laurel biodiesel. In Energy Recovery Processes from Wastes (pp. 51-63). Springer, Singapore.

[149]. Sindhu, Binod, P., & Pandey, A. (2015). Microbial Poly-3-Hydroxybutyrate and Related Copolymers. In Industrial Biorefineries and White Biotechnology (pp. 575–605).

[150]. Ishiyama, M., Miyazono, Y., Sasamoto, K., Ohkura, Y., & Ueno, K. (1997). A highly water-soluble disulfonated tetrazolium salt as a chromogenic indicator for NADH as well as cell viability. Talanta, 44(7), 1299-1305.

[151]. McKinnon K. M. (2018). Flow Cytometry: An Overview. Current protocols in immunology, 120, 5.1.1–5.1.11.

[152]. Adan, A., Alizada, G., Kiraz, Y., Baran, Y., & Nalbant, A. (2017). Flow cytometry: basic principles and applications. Critical reviews in biotechnology, 37(2), 163-176.

[153]. Macey, M. G., & Macey, M. G. (2007). Flow cytometry. Humana Press Incorporated.

[154]. Zharov, V. P., Galanzha, E. I., Shashkov, E. V., Kim, J. W., Khlebtsov, N. G., & Tuchin, V. V. (2007). Photoacoustic flow cytometry: principle and application for real-time detection of circulating single nanoparticles, pathogens, and contrast dyes in vivo. Journal of biomedical optics, 12(5), 051503.

[155]. Paddock, S. W. (1999). Confocal laser scanning microscopy. Biotechniques, 27(5), 992-1004.

[156]. Tata, B. V. R., & Raj, B. (1998). Confocal laser scanning microscopy: Applications in material science and technology. Bulletin of Materials Science, 21(4), 263-278.

[157]. Kuehn, M., Hausner, M., Bungartz, H. J., Wagner, M., Wilderer, P. A., & Wuertz, S. (1998). Automated confocal laser scanning microscopy and semiautomated image processing for analysis of biofilms. Applied and environmental microbiology, 64(11), 4115-4127.

[158]. Kim, K., Lee, S., Jin, E., Palanikumar, L., Lee, J. H., Kim, J. C., ... & Ryu, J. H. (2019). MOF× biopolymer: collaborative combination of metal–organic framework and biopolymer for advanced anticancer therapy. ACS applied materials & interfaces, 11(31), 27512-27520.

Appendix

Abbreviation

Acronym	Full name
MOF	Metal organic framework
EPR	Enhanced permeation retention effect
PDT	Photodynamic therapy
ROS	Reactive oxygen species
FA	Folic acid
FR	Folate receptor
MTX	Methotrexate
CPP	Cell penetrating peptide
H	Histidine
R	Arginine
K	Lysine
NP1	Stearyl-H16R8-NH2
NPKMTX	Stearyl-H16R8K-MTX
Dox	Doxorubicin
TCPP	Tetra(4-carboxyphenyl) porphyrin
PCN	porous coordination network
DP	Dox@PCN-224
PN	PCN-224-NPKMTX
DPN	Dox@PCN-224-NPKMTX
DLS	Dynamic light scattering
CDs	Circular dichroism spectroscopy
CAC	Critical aggregating concentration

AFM	Atomic force microscopy
SEM	Scanning electronic microscopy
FTIR	Fourier-transform infrared spectroscopy
FACS	Fluorescence-activated cell sorting
CLSM	Confocal laser scanning microscope
MW	Molecular weight
CQD	Carbon quantum dots
CCK8	Cell count kit 8
PSs	Photosensitizers
TME	Tumor microenvironment
EPT	Ellipticine
BA	Benzoic acid
DMF	Dimethylformamide
ABDA	9,10-Anthracenediyl-bis(methylene)-dimalonic acid
FBS	Fetal bovine serum
PBS	Phosphate-buffered saline
PFA	Paraformaldehyde
GSH	Glutathione
XPS	X-ray photoelectron spectroscopy
ITC	Isothermal titration calorimetry
DFT	Density functional theory